Advanced Steel Construction – Vol. 21 No. 2 (2025) 95–109
DOI:10.18057/IJASC.2025.21.2.1

AXIAL COMPRESSION BEHAVIOR OF DOUBLE-SKIN COMPOSITE SHEAR WALL WITH T-STIFFENER AND HEADED STUD CONNECTORS

Mohammed Amer [1, *], Zhi-Hua Chen [1, 2, 3], Yan-Sheng Du [1, 2, 3, *], W. A. H Mashrah [4] and Saleh Ahmad Laqsum [1]

[1] *School of Civil Engineering, Tianjin University, Tianjin, 300072, China*
[2] *Key Laboratory of Coast Civil Structure Safety of Ministry of Education, Tianjin University, Tianjin, China*
[3] *State Key Laboratory of Hydraulic Engineering Intelligent Construction and Operation, Tianjin University, Tianjin, China*
[4] *Dali Construction Group Co., Ltd, Hangzhou, 310000, China*
** (Corresponding author: E-mail: amer@tju.edu.cn; duys@tju.edu.cn)*

ABSTRACT

Double-skin composite shear walls (DSCSWs) offer high strength and improve construction processes in tall structures, offshore constructions, and nuclear power plants. This paper investigates the compressive performance of DSCSWs, which consist of concrete sandwiched between two external steel faceplates and bonded with connectors at regular intervals. Three-dimensional finite element (FE) modeling is established and verified against five axial compression test specimens to predict the ultimate compressive capacity and failure modes of DSCSWs with bolts, head studs, and T-stiffener connectors. Parametric studies evaluate the impact of five factors on the compressive performance of DSCSWs. The results show that different connectors provide confinement to the concrete core, enhancing the compressive capacity of DSCSWs, with T-stiffeners being the most effective. Furthermore, variations in the thickness of the steel plates, concrete core, and height of the walls significantly affect the strength and ductility of DSCSWs, while changes in bolt spacing have insignificant effect. Finally, the ultimate compressive capacity of DSCSWs is calculated using code equations and an analytical method. The prediction results show a good correlation with the numerical results. These findings provide valuable insights for implementing DSCSWs in engineering applications, particularly in design for practical use.

ARTICLE HISTORY

Received: 12 August 2024
Revised: 18 December 2024
Accepted: 20 December 2024

KEYWORDS

Double-skin-composite shear wall (DSCSW);
Compressive performance;
T-stiffener connector;
Local buckling;
Finite element modeling (FEM)

1. Introduction

Over the past few decades, reinforced concrete (RC) shear walls have been the primary structural element to resist lateral forces in tall structures, supporting vertical and horizontal loads. Despite their widespread use, RC shear walls have several drawbacks, including limited ductility, susceptibility to cracking, considerable thickness, and complex construction requirements [1-4]. To enhance the performance of shear walls, researchers have proposed various composite shear walls including steel plate shear walls [5-8], concrete-encased profile steel composite shear walls [9], steel plate-reinforced concrete shear walls [10] and double steel plate composite shear walls (DSCSWs) [11-14]. Among these, the double steel plate DSCSWs is particularly advantageous due to its superior performance, reduced wall thickness, and potential for prefabrication. This type of DSCSWs consists of two steel plates on the surface, with concrete sandwiched in between, and the steel plates are connected to the concrete using different shear connectors. To improve the bond between steel plates and concrete, researchers have explored various types of shear connectors, including welded stiffeners [15], welded short studs [16], welded or mechanical pulling bars [17, 18], welded trusses [19], and specially designed connectors [20]. These types of connectors aim to increase the bold interactions between steel plates and concrete core, preventing the local buckling and improve the compressive capacity of walls [21-23]. The DSCSWs has many applications such as nuclear power plant walls, offshore walls, offshore constructions, urban roads, bridges, shield tunnels, military shelters [22-27].

This study focuses on DSCSWs constructed with thin-walled steel plates. The shear studs, which are commonly employed as connectors in conventional DSCSWs, are recognized for their straightforward manufacturing process and robust connection performance. Research by Choi et al. [28] and Fan et al. [29] explored the behavior of DSCSWs subjected to axial compression with shear stud connectors. Their findings revealed that the primary failure mechanism in these structures under axial loads is the local buckling of the steel plates. Yan et al. [30] examined the performance of DSCSWs connected with shear studs of varying lengths under axial compression. They discovered that while increasing shear stud length improved the axial load capacity, it had minimal impact on the localized buckling characteristics of the steel plates. On the other hand, Nie et al. [15] evaluated DSCSWs incorporating stiffeners and batten plate connectors, finding that the combination of shear studs with other types of connections could effectively reduce local buckling. This indicates that pairing shear studs with alternative connection designs can enhance the resistance to local buckling in thin-walled steel plate DSCSWs.

Several researchers have proposed novel designs incorporating profiled steel components to improve both the assembly process and mechanical performance of DSCSWs. Chen et al. [31, 32] introduced a DSCSW utilizing C-shaped steel units, while Guo et al. [32] and He et al. [33, 34] recommended the use of H-shaped and L-shaped steel units, respectively. These innovations help reduce the width-to-thickness ratio of the steel face plates, enhancing steel-concrete interaction and increasing stiffness due to the structural stability of the cross-sectional shapes. Moreover, these profiled steel units can act as formwork for concrete pouring, offering cost savings in construction. The standardization of these units also paves the way for increased industrial production. However, there are challenges with C- and H-profiled steel units, as shear connectors cannot be welded into their narrow web flanges, and L-profiled units require significant welding during assembly. To overcome these challenges, a new DSCSW design featuring Z-profiled steel units with shear studs welded into the flange has been proposed [11-13, 35, 36]. Studies examining the cyclic and axial compression performance of these DSCSWs, using iron tiling recycled aggregate concrete revealed that the cyclic tests exhibited strong bearing capacity, stiffness, and energy dissipation, suggesting that iron tiling recycled aggregate concrete could serve as a viable alternative to traditional concrete. The axial compression tests indicated that incorporating shear studs improved both the axial bearing capacity and initial stiffness. However, increasing the spacing of the inner diaphragm led to a decrease in axial bearing capacity, initial stiffness, and ductility. On the other hand, increasing the height-to-thickness ratio significantly enhanced both initial stiffness and ductility, with minimal impact on bearing capacity.

Since the time and cost of conducting testing program, the finite element technique becomes more used and offers alternative methods to analyze structural performance [14, 37-40]. FE modeling provides acceptable results and a practical approach to simulating different parts of the DSCSWs, with complicated interactions among concrete slab, steel plates and connections, different load and boundary conditions, and different grade materials. Former researchers concentrated on the push-out shear tests of headed connectors [41-45]. On the other hand, a series of numerical investigations on structural performance on DSCSWs with ultra-lightweight concrete, cementitious materials, including several parameters and types of connectors, were developed and compared with experimental results [20, 27, 43, 46], resulting to a great understanding on the impact of key factors that might impact the structural performance which can lead to the implementation to researcher and designers. FE modeling analysis was also used to simulate the load-deflection curves, ultimate compressive capacity, and deformation patterns of the walls, and experimental and numerical results proved that all the proposed equations could be used for the design of DSCSWs with all types of connectors [46]. Yan et al. [47] proposed a three-dimensional damage plasticity-based FE model to simulate the ultimate compressive capacity of DSCSWs subjected to axial load. The concrete damage plasticity model (CDPM) was used to simulate the ultimate capacity of the concrete, and the continuum damaged model (CDM)

was also used to simulate the evolution of steel materials. The results showed that the FE model provided reliable estimations of ultimate strength, load-deflection behavior, and failure modes in Steel-concrete-steel sandwich plates, offering a useful tool for analyzing steel-composite structures with mechanical shear connectors.

This study focuses on the compressive behavior of DSCSWs using bolts, headed studs, and T-stiffener connectors. The ultimate axial load-bearing behavior of walls incorporating normal-weight concrete is investigated. FE models were developed using ABAQUS CAE software to study the compressive behavior and failure modes. The FE modeling findings were verified against five tested specimens to enhance the reliability of the findings. This study also examines the impact of various factors on the ultimate compressive capacity, initial stiffness, ductility index, and ultimate vertical displacement of DSCSWs. Additionally, calculation methods from AISC 360, Eurocode 4, and analytical approaches are included to predict the ultimate axial bearing capacity, with a comparison to the FE modeling results.

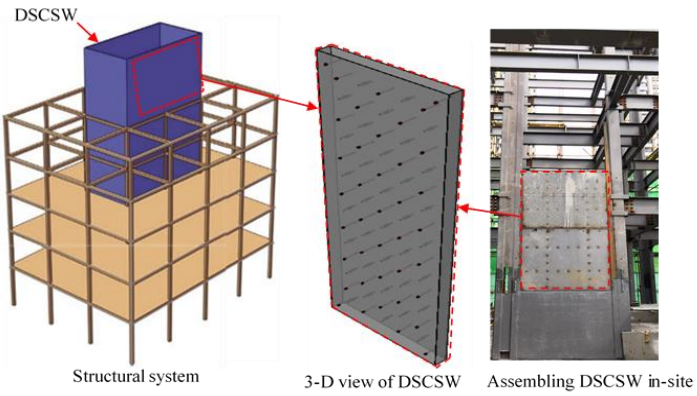

(a) High-rise buildings

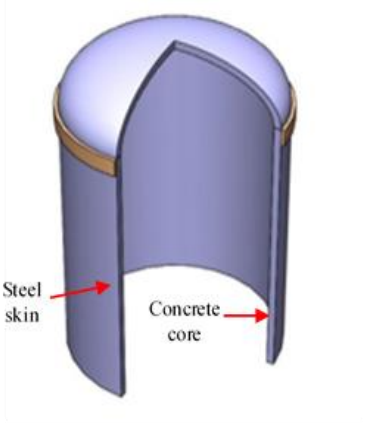

(b) Nuclear power plant

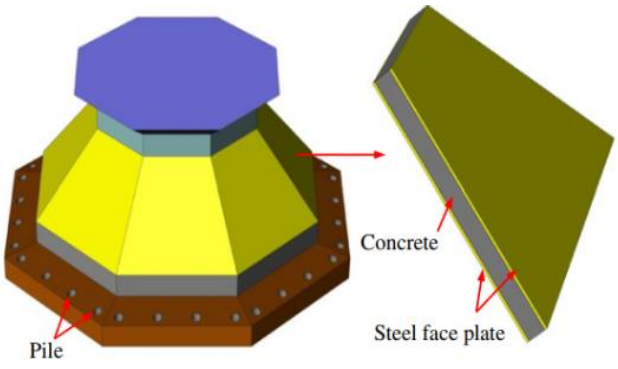

(c) DSCSW in protective Arctic offshore constructions

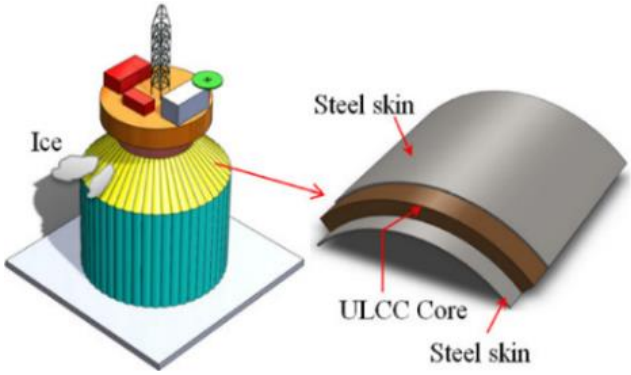

(d) Conical Arctic structure

Fig. 1 Applications of DSCSW in different structures

2. Experimental program

2.1. Specimen design

A total of five specimens were created and tested to examine the axial compression performance of DSCSWs. Each specimen consisted of four primary components: a concrete core, steel faceplates, side steel plates, and connectors, as illustrated in Fig. 2(a-e). Specimen W1 had a height of 600 mm, while specimens W2, W3, W4, and W5 were designed with heights of 1500 mm and 3000 mm to investigate the effect of height on DSCSW performance. The steel faceplate and concrete core thicknesses were kept constants for all specimens at 6 mm and 118 mm for all specimens, respectively. Three types of connectors were used in this study: bolts, headed studs, and T-stiffeners, as depicted in Fig. 2(c-e). The detailed specifications of the specimens are provided in Table 2, which presents the geometric dimensions, including length, height, width, steel plate thickness, concrete core thickness, connector spacing, and connector types.

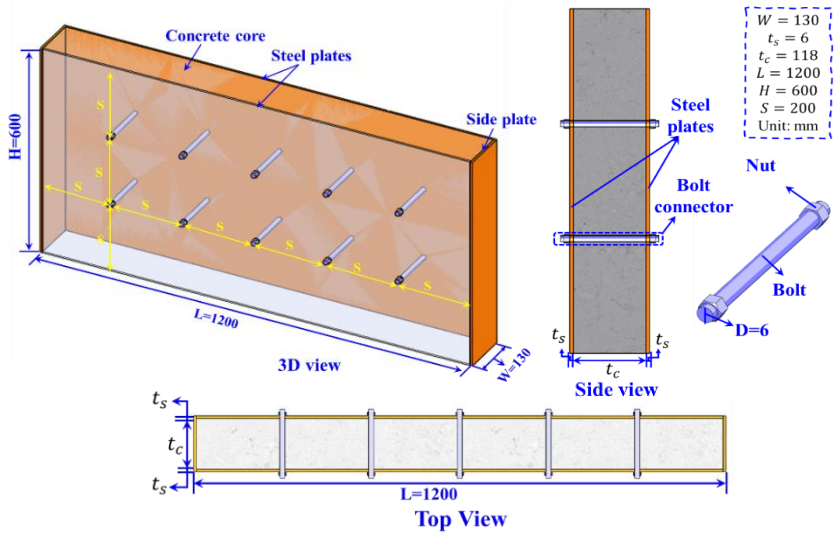

(a) W-1

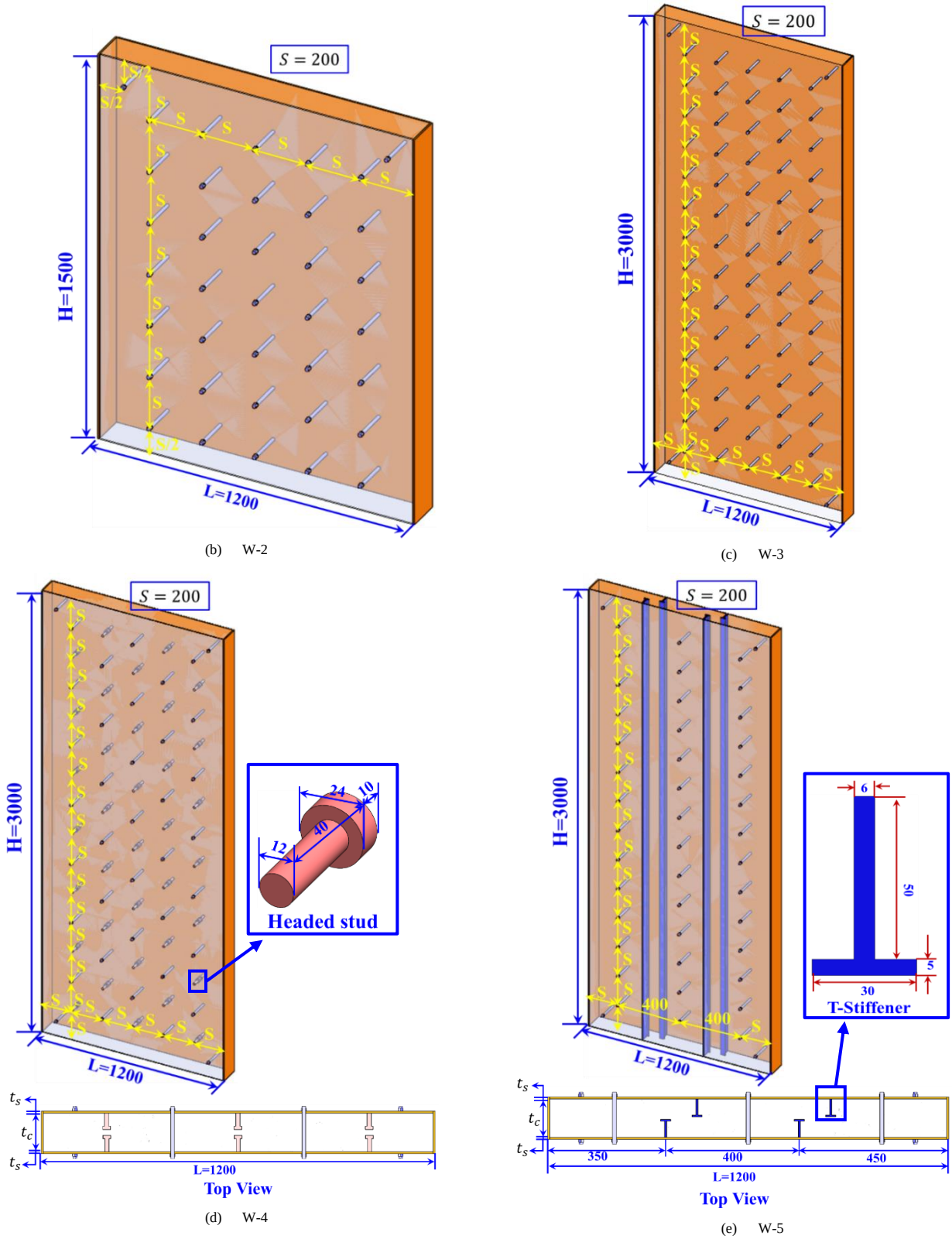

Fig. 2 Details of DSCSW with different types of connectors

Table 1
General details of the specimens

Specimens ID	L (mm)	H (mm)	w (mm)	H/w	t_s (mm)	t_c (mm)	S (mm)	S/t_s	Type of connectors
W-1	1200	600	130	4.62	6	118	200	33.33	Bolts
W-2	1200	1500	130	11.08	6	118	200	33.33	Bolts
W-3	1200	3000	130	23.08	6	118	200	33.33	Bolts
W-4	1200	3000	130	23.08	6	118	200	33.33	Bolts & headed stud
W-5	1200	3000	130	23.08	6	118	150/200/250	33.33	Bolts &T-Stiffeners

where $L, H, and\ w$ indicate to the length, height and width of the wall respectively, $t_s\ and\ t_c$indicate the thickness of steel plates and thickness of concrete core respectively, S indicates the spacing between connectors

2.2. Materials properties

The concrete cubic blocks, with dimensions of 100 × 100 × 100 mm, were tested in accordance with the GB/T50081-2010 standard [48]. The average compressive strength of the concrete was 28.57 MPa, with a Young's modulus of 31.6 GPa. Q355 steel was adopted for the manufacture of steel plates and T-stiffeners. Table 2 lists the results of three coupons of the same thickness that were prepared and tested, including the yield strength and ultimate strength.

Table 2
Test results in steel material properties

Thickness (mm)	Yield strength (MPa)	Ultimate strength (MPa)	Modulus of Elasticity (GPa)
6 (Steel plate)	345.32	522.50	186
5 (stiffener)	366.49	470.53	193

2.3. Test setup

Fig. 3 shows the testing setup for DSCSWs under in-plane compression load. It demonstrates that all specimens were positioned directly on a rigid support to simulate the fixed support at the bottom loading plate, using a 1500-ton MTS testing machine. The loading procedure was divided into two phases: pre-loading and formal loading. During the pre-loading phase, 10% of the ultimate load was applied, held for 5 minutes, and then unloaded to zero. This ensured proper contact between the specimens and the loading apparatus and confirmed the measuring instruments' functionality. In the formal loading phase, the load gradually increased at the same rate as in the pre-loading phase until the ultimate bearing capacity of the wall was reached. After achieving the compressive capacity, significant visible deformation was observed. The concrete cracking and buckling of the steel plates were recorded during each loading stage.

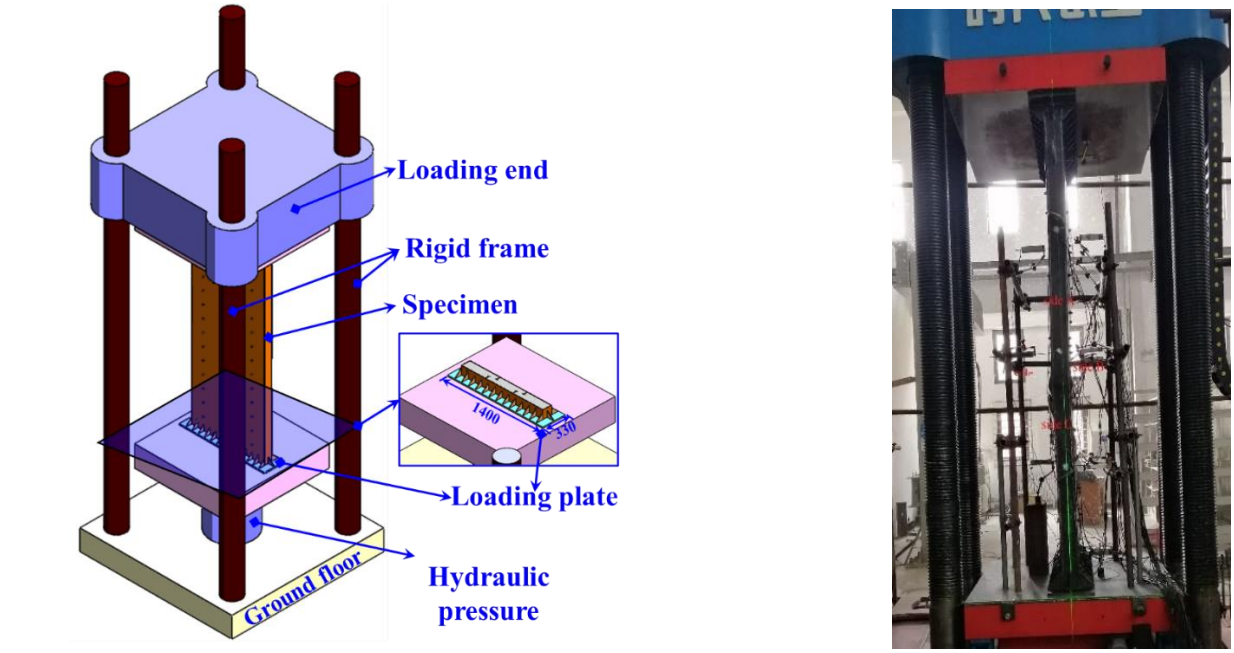

(a) 3-D diagram of testing setup

(b) Loading process in laboratory

Fig. 3 Testing machine and test setup

3. Finite element model on DSCSWs

Based on experimental investigations cited in reference [49], FE models were established in ABAQUS/standard [50] to investigate the compressive behavior and structural stability of DSCSWs under axial compression load. Geometrical, material nonlinearities, meshing convergence, the complexity of contact, loading, and boundary conditions were considered. Parametric studies were elaborated to comprehend the effect of key parameters on the compressive behavior of DSCSWs, including types of connectors, height of the wall, steel plates' thickness, bolt connectors' spacing, and thickness of the concrete core. The details of FE models are listed in Table 3.

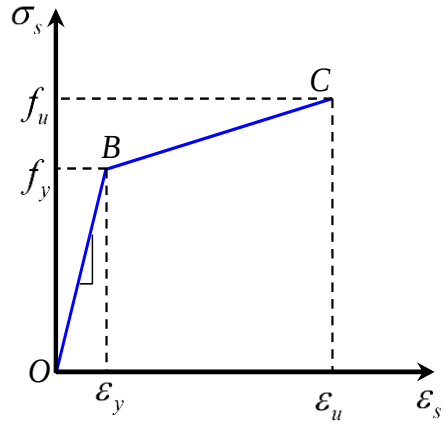

Fig. 4 Stress-Strain steel material model

3.1. Material model

3.1.1. Steel model

A nonlinear isotropic/kinematic hardening model was used to simulate all steel elements. The von Mises yield criterion was applied to represent the isotropic yielding of all components in the FE model. The model exhibited bi-linear behavior with strain hardening, as illustrated in Fig. 4. The values for the modulus of elasticity, yield strength, and ultimate strength are provided in Table 2.

3.1.2. Concrete constitutive

The Concrete Damage Plasticity Model (CDPM), a continuum and plasticity-based damage model in ABAQUS, is used to simulate the core concrete of the DSCSW. Two deformations methods are considered: compressive crushing and tensile cracking of the concrete. The compressive stress-strain curve for C30 concrete was gotten according to GB50010-2010 [51], which was adopted to standardize the input data for compressive stress versus inelastic strain ($\tilde{\varepsilon}_c^{in}$), as shown in Fig. 5(a). For compressive behavior, the stress-strain response of plain concrete in uniaxial compression outside the elastic range can be stated using plasticity and damage parameters. Unloading data is provided in CDPM based on compressive damage curves [50], as described by the following equation.

$$\tilde{\varepsilon}_c^{pl} = \tilde{\varepsilon}_c^{in} - \frac{d_c}{(1-d_c)}\frac{\sigma_c}{E_0} \quad (1)$$

where $\varepsilon_c^{el} = \frac{\sigma_c}{(1-d_c)E_0}$ which is defined as the difference between total strain ε_c and plastic strain $\tilde{\varepsilon}_c^{pl}$; $\tilde{\varepsilon}_c^{el}$ is the elastic strain corresponding to the undamaged materials with $\tilde{\varepsilon}_c^{el} = \frac{\sigma_c}{E_0}$, which is equal to $\varepsilon_{0c}^{el} = \varepsilon_c - \tilde{\varepsilon}_c^{in}$; $\tilde{\varepsilon}_c^{in}$ is the inelastic strain instead of plastic strain $\tilde{\varepsilon}_c^{pl}$, by which ABAQUS automatically converts the inelastic strain values $\tilde{\varepsilon}_c^{in}$ to plastic strain values $\tilde{\varepsilon}_c^{pl}$. Besides, σ_c denotes the uniaxial compressive stress, and E_0 denotes young's modulus. For tensile behavior, ABAQUS automatically converts the inelastic strain to plastic strain. As shown in Fig. 5.(b), unloading data can be given in CDPM based on the tensile damage curve expressed by the following equation.

$$\tilde{\varepsilon}_t^{pl} = \tilde{\varepsilon}_t^{ck} - \frac{d_t}{(1-d_t)}\frac{\sigma_t}{E_0} \tag{2}$$

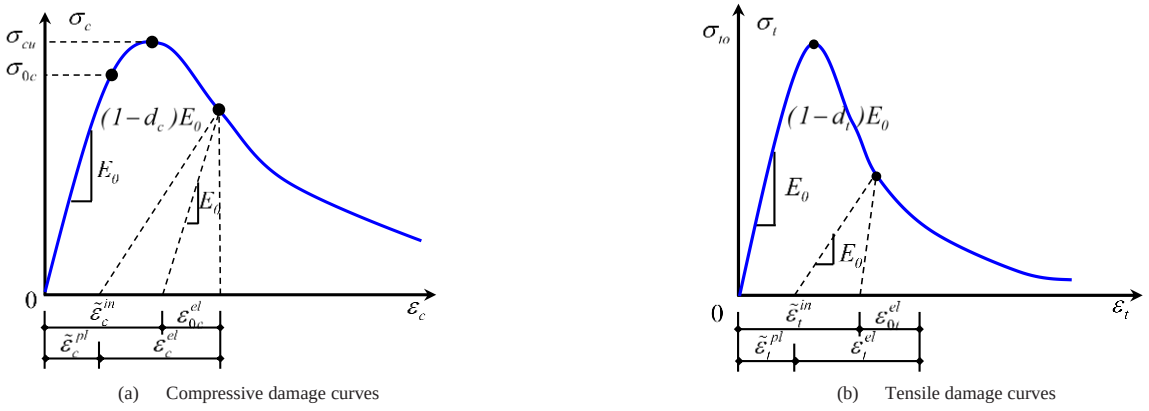

(a) Compressive damage curves (b) Tensile damage curves

Fig. 5 Damage curves of concrete

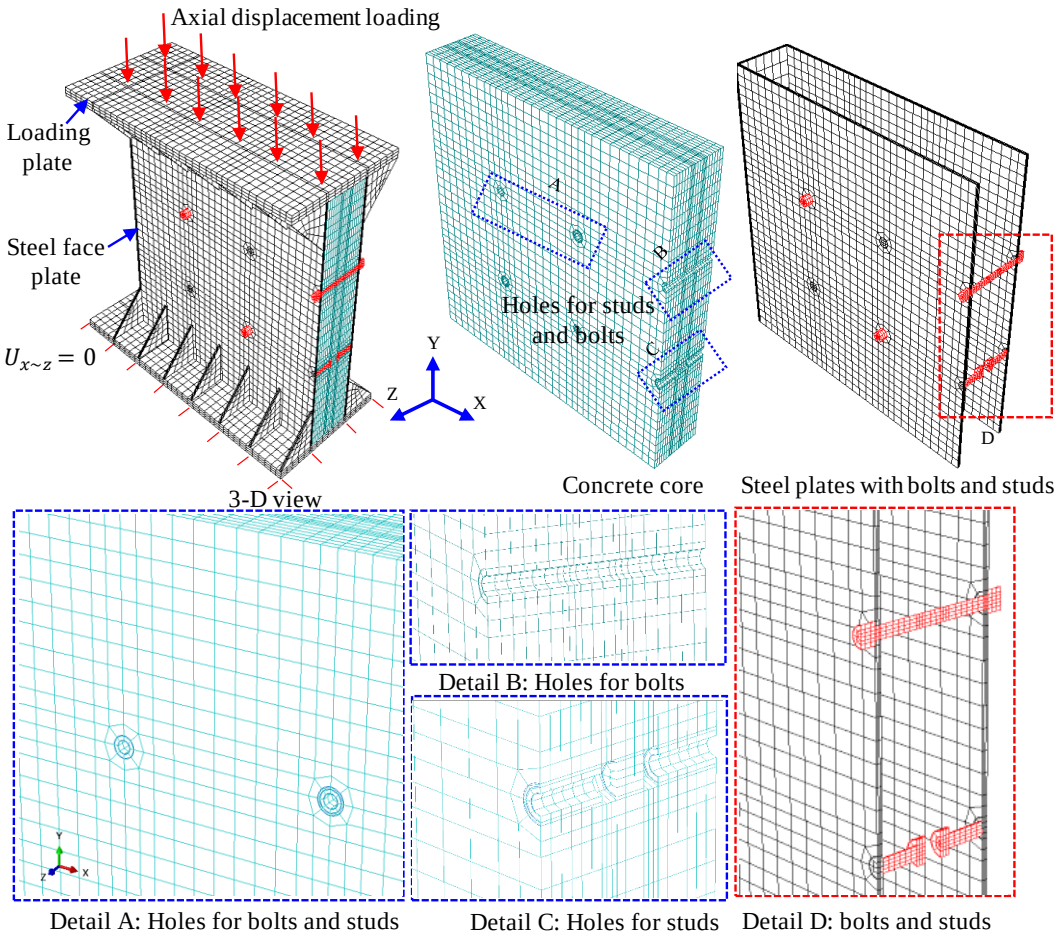

Fig. 6 Typical finite element model for DSCSW

3.2. Element mesh and interactions

ABAQUS/CAE offers a wide range of element types, including link, beam, connection, solid, thin-film, and infinite elements. An eight-node solid element with reduced integration (C3D8R) was selected to model all components, including the loading plates, steel plates, concrete core, bolts, headed studs, and T-stiffener connectors [47, 52-54]. A series of mesh sensitivity considers were performed to balance the accurateness of the FE model with computational efficiency. As a result, the general mesh size for all elements was set to 20mm, except for the bolts and headed studs, which were meshed with sizes of 10mm and 4mm, respectively. The geometry of the DSCSW node is generally symmetrical, and for a more detailed simulation, the connectors were explicitly modeled. Holes were incorporated in the steel plates and concrete core to accommodate the connectors, as shown in Fig. 6.

The contact relationship of the DSCSW wall's node model is defined as frictional contact. A surface-to-surface contact algorithm was used to model the interactions among various elements of the DSCSW, including the bolts, headed studs, T-stiffeners, the concrete core and the steel plates. The contact surfaces

were defined based on the material hardness, with the bolts, headed studs, T-stiffeners, and steel plates elected as the master surface, and the concrete core selected as the slave surface. The contact algorithm allows penetration of the master surface into the slave surface, but not the reverse. The interaction properties account for the transfer of forces in both the tangential and normal directions at the steel-concrete interface. In the tangential direction, "penalty friction" was used to simulate the frictional force between the concrete and steel, with a friction coefficient of $\mu = 0.4$ [37, 55]. Additionally, a tie constraint was applied to simulate the welding behavior of the steel plates.

3.3. Loading process and boundary conditions

The axial load was applied as a point displacement load on the top loading plate, with a coupling constraint created between the loading point and the surface of the loading plate. The load was applied in two steps. The first step represented the pre-loading phase in the experiments, while the second step represented the main loading phase. The point load was considered as the master surface, and the loading plate surface was treated as the slave surface. The point load was constrained to prevent movement in any direction, while the bottom plate surface was also constrained from moving in any direction [54, 56, 57]. Symmetrical restraints were applied to the corresponding surface in the FEM, as shown in Fig. 6.

3.4. Validations of FE models

Fig. 7(a-e) presents a comparison of the load-displacement behavior between the experimental and FE modeling results. Table 4 summarizes the comparison of the ultimate compressive capacity, initial stiffness, and ductility index between the experimental and FE results. The FE models tend to slightly overestimate both the ultimate compressive capacity and initial stiffness of DSCSWs by about 7%, with standard deviations of 0.06 for the ultimate compressive capacity and 0.04 for initial stiffness. The ductility predicted by the FE models is highly accurate, although it shows a minor overestimation of 2%. The small discrepancies observed for specimens W-2 and W-3, where the FE modeling calculates higher ultimate compressive capacity and stiffness than the experimental data, could be attributed to factors such as manufacturing imperfections, variations in the concrete's modulus of elasticity, or differences in the loading process. Overall, the FE models demonstrate good accuracy for all parameters, indicating their reliability for further parametric studies on the compressive behavior of DSCSWs.

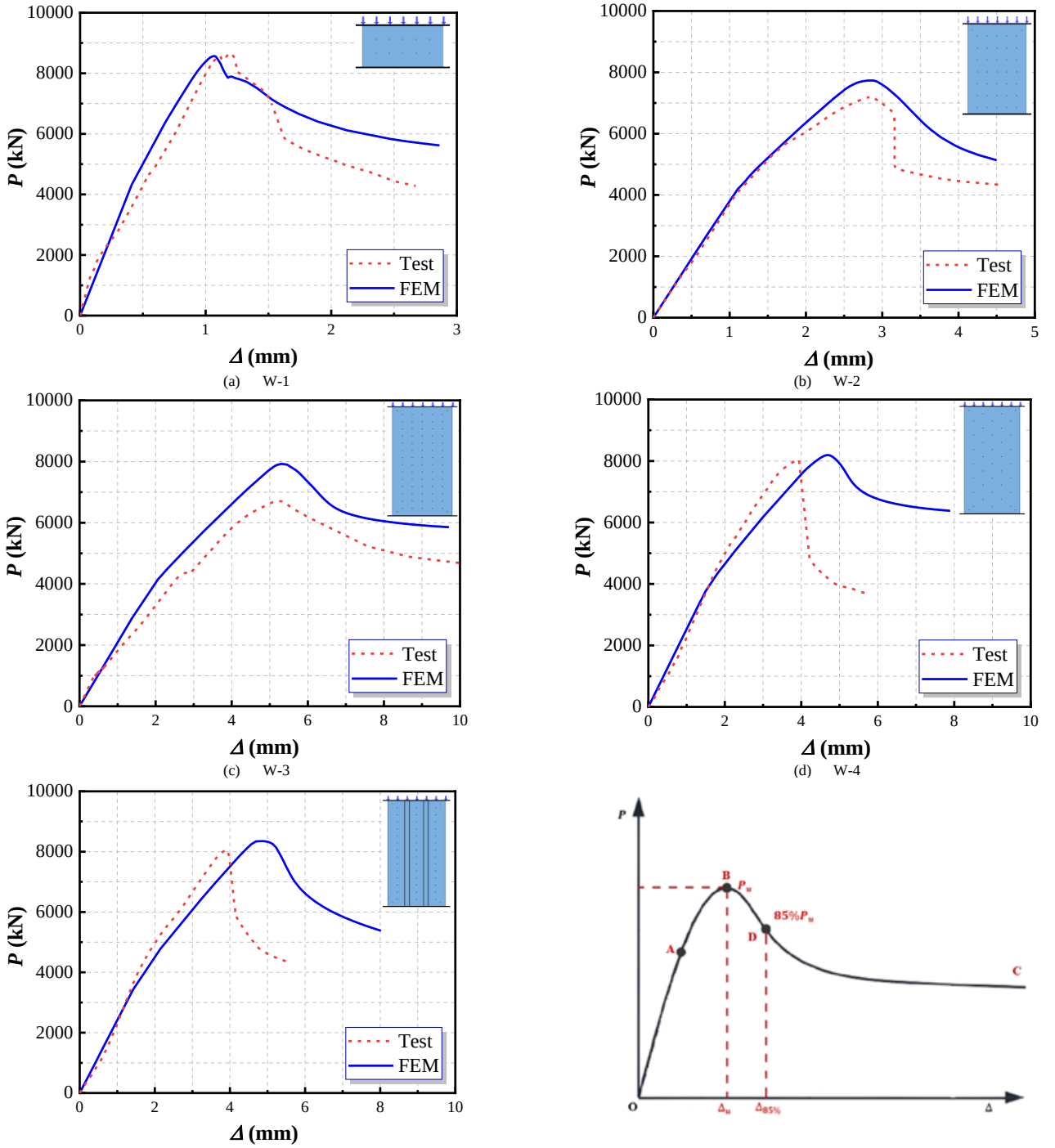

Fig. 7 Experimental and FE modeling of load-displacement curves (P − Δ) of DSCSW

Table 3
Accuracy of FE modeling results

`	$P_{u,FEM}$ (kN)	$P_{u,FE}$ (kN)	$\frac{P_{u,Test}}{P_{u,FE}}$	$K_{e,Test}$ (kN/mm)	$K_{e,FE}$ (kN/mm)	$\frac{K_{e,Test}}{K_{e,EFM}}$	DI_{Test}	DI_{FEM}	$\frac{DI_{Test}}{DI_{FEM}}$
W-1	8659	8870	0.98	9845	10424	0.94	1.20	1.35	0.94
W-2	7200	8226	0.88	3595	4054	0.89	1.12	1.21	0.93
W-3	6735	7853	0.86	1797	2088	0.87	1.31	1.18	1.11
W-4	8060	8191	0.98	2308	2406	0.96	1.17	1.19	0.98
W-5	8063	8350	0.97	2342	2413	0.93	1.13	1.15	0.98
average			0.93			0.93			0.98
Std.v			0.06			0.04			0.07

where H/w denotes the ratio of height to width of the specimens; $P_{u,Test}$ and $P_{u,FEM}$ denote the compressive capacity from experimental and FE modeling , respectively; $K_{e,Test}$, $K_{e,FEM}$ denote the initial stiffness from experimental and FE modeling , respectively. DI_{Test} and DI_{FEM} are the ductility index that obtained from test and FE modeling.

Fig. 8(a-e) compares the deformation patterns between the FE models and the experimental results. steel plates' local buckling was observed and compared for specimens W-1 and W-2. However, the FE models were not able to precisely capture the local buckling, likely due to uncertainties in the initial imperfections of the steel plates and the tensile fracture at the welds connecting the steel faceplates to the side plates. Generally, The FE modeling provide an acceptable results in term of the failure modes and deformation patterns.

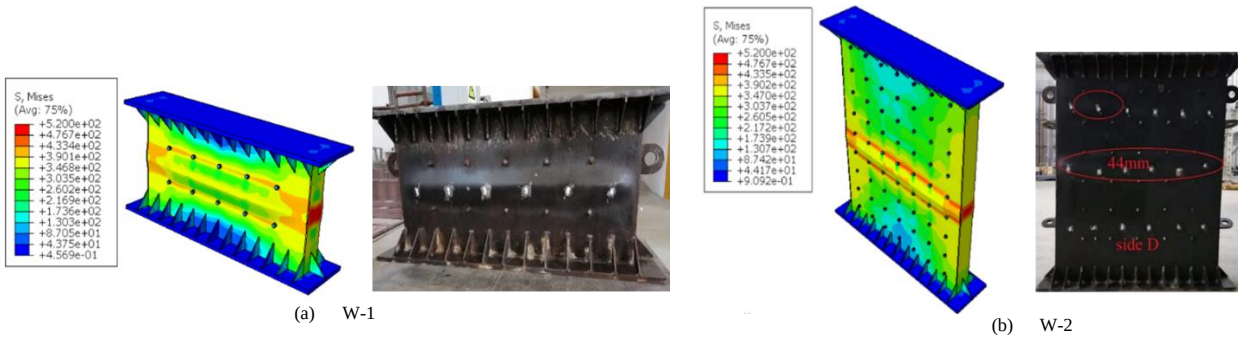

(a) W-1 (b) W-2

Fig. 8 Comparison of failure modes between test results and FE modeling

4. Results and discussions

4.1. General behavior

Fig. 7(a–f) shows the axial compression load versus vertical displacement (P-Δ) curves for the five DSCSW models. Based on experimental investigations, the load-displacement curves can be divided into three stages: the elastic stage, the non-linear elastic stage, and the degradation stage. In the first stage (curve OA), the curve is nearly linear, indicating that the displacement increases proportionally with the load, and the specimens achieve 50%-85% of their ultimate capacity, as shown in Fig. 7(f). In the second stage (curve AB), the DSCSWs exhibit non-linear behavior due to the material non-linearities of concrete, steel plates, and connectors. At the end of this stage (point B), the models reach their ultimate capacity. Finally, the degradation stage (curve BC) begins, where the load capacity declines. The rate of decline depends on the type of connectors and the height of the DSCSWs. For instance, the ultimate resistance of DSCSWs decreases with height but increases when bolts are replaced with headed studs and T-stiffeners (see Fig. 7).

4.2. Ductility index (DI)

In structural stability, the ductility index reflects the capability to experience significant plastic failure without essential capacity breakdown. The following equation can determine the ductility index.

$$DI = \frac{\Delta_{0.85}}{\Delta_u} \tag{3}$$

where $\Delta_{0.85}$ indicates the shorting reaction force of DSCSW declined to its 85% ultimate value during the recession stage; Δ_u indicates the shorting corresponding to ultimate capacity.

4.3. Initial stiffness

The initial stiffness K_e of the compression behavior of DSCSW can be determined based on [58] method from the load-displacement curve, using the ratio of 30% from ultimate axial compassion resistance $P_{0.3}$ and its corresponding displacement as the following equation.

$$K_e = \frac{P_{0.3}}{\Delta_{0.3}} \tag{4}$$

where K_e denotes the initial stiffness of DSCSW based on numerical analysis.

In addition, the initial stiffness of DSCSW subjected to an axial load can be calculated based on the equation as follows.

$$K_{ca} = \frac{E_c A_e}{H} \tag{5}$$

$$A_e = A_c + A_s(E_s/E_c) \tag{6}$$

where K_{ca} denotes initial theoretical stiffness of DSCSW, E_s and E_c denote the elastic modules and of concrete and steel plates, respectively, H is the height of the wall, A_e is the equivalent area of cross-section of the DSCSW, A_c and A_s denote the total area of concrete core and steel plates, respectively.

Fig. 9 shows the scattering distributions of initial theoretical stiffness K_{ca}. It can be noticed that theoretical predictions of initial stiffness are overestimated by 13% with stander deviations due to only considering the capacity and height of the material without different types of connectors.

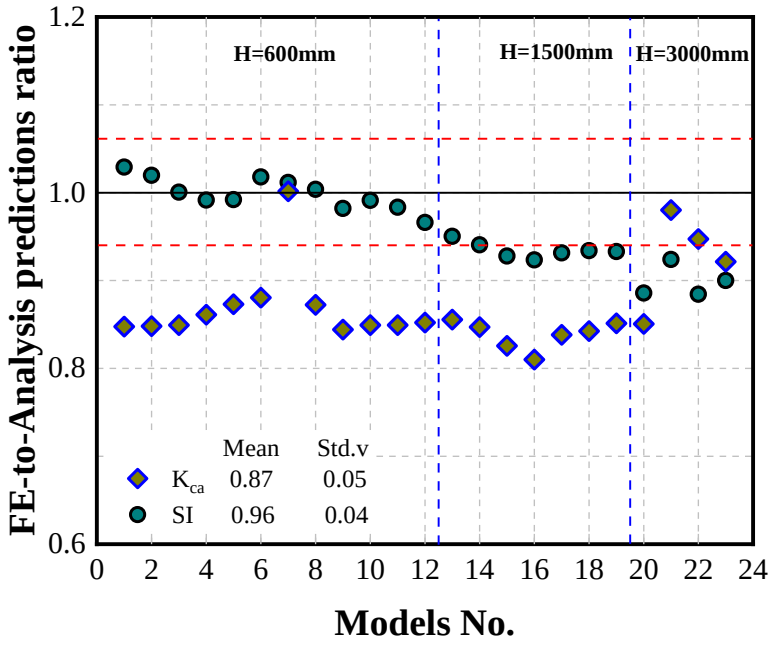

Fig. 9 Scatter of FE-to-predictions of (K_{ca}) and (SI)

4.4. Strength Index (SI)

In order to eliminate the variation of models' sectioned configurations and height, the strength index is proposed, which is able to be determined as the following.

$$SI = \frac{P_{u,FEM}}{0.85 f_c A_c + f_y A_s} \tag{7}$$

where SI is the strength index of the DSCSW subjected to compression load; $P_{u,FEM}$ is the ultimate compressive capacity based on FE analysis; f_c and A_c indicate the yield strength and cross-sectional area of the concrete core; f_y and A_s indicate the yield strength and cross-sectional area of steel plates.

The scatter distribution of the strength index ratio is illustrated in Fig. 9. It is noticeable that the ratio was close to the linear fitting, which means the wall's ultimate compressive capacity takes the full section capacity. However, the ultimate compressive capacity tends to decrease with the height of the wall being raised. This exhibits that the shear wall cannot achieve its section capacity due to premature failure, which causes local bucking, concrete crushing, and global buckling. Additionally, the mean ratio value of the strength index is 96% with standard deviations (Std.v) 0.04.

4.5. Ultimate compressive capacity and failure modes

4.5.1. Ultimate compressive capacity

The ultimate compressive capacity of FE models can be calculated from load-displacement curves as presented in Table.4. Test results revealed that increasing the wall height led to a decrease in ultimate compressive capacity, initial stiffness, and ductility, while vertical displacement increased. Specifically, at a wall height of 600mm, the ultimate bearing capacity was 8659kN, but it decreased to 7200kN and 6735kN for heights of 1500mm and 3000mm, respectively. The initial stiffness was 9845 kN/mm, then declined by roughly 37% and 18% when the height increased from 600mm to 1500mm and 3000mm, respectively. The ductility index was 1.20%, 1.12%, and 1.31%, with heights changing from 600mm to 1500mm and 3000mm. Therefore, height is a significant factor influencing the overall performance of the DSCSWs.

Using different types of connectors showed that both compressive capacity and initial stiffness increased with the use of headed studs and T-stiffeners, while the ductility index and vertical displacement exhibited the opposite behavior. Specifically, the axial bearing capacity increased from 6735kN to 8060kN and 8063kN when bolt connectors, headed studs, and T-stiffeners were used. Initial stiffness was 1759kN/mm with bolt connectors, and it increased by 76% with both headed studs and T-stiffeners, as shown in the table. 4. The ductility index showed minimal variation, the ductility index was 1.31% with bolt connectors, then declined to 1.17% and 1.13% with the use of headed studs and T-stiffeners, respectively. Overall, the axial bearing capacity, stiffness, and ductility index of the DSCSWs are primarily influenced by the steel faceplate and material resistance of the wall. Headed stud and T-stiffener connectors outperformed bolt connectors and are recommended for enhancing the overall performance of the DSCSWs.

4.5.2. Failure modes

Three main styles of deformation patterns were observed in the FE simulation of compression tests of DSCSWs. The first failure mode, concrete crushing deformation, is described by the high yielding of the concrete core between two vertical connectors, where the concrete tends to crush, as depicted in Fig. 10(a). This type of deformation occurs due to the straight growth of the concrete core under axial compression. The excessive axial load causes the concrete to reach its compressive limit, leading to localized crushing. This failure mode emphasizes the need for sufficient confinement within the wall system to prevent premature crushing and improve the axial load capacity. The second failure mode is steel faceplate buckling, as presented in Fig. 10(b-c). In this case, the steel faceplates tend to buckle outward in the middle due to insufficient connections between the concrete core and the steel plates. This poor connection allows the steel plates to deform, resulting in a deformation strip zone along the shear connectors. The confinement effect afforded by the steel faceplates is crucial for enhancing the compressive capacity of the concrete core. By improving the steel-concrete interface and using effective connectors, the ultimate capacity of DSCSWs can be significantly increased, as evidenced by the absence of this failure mode in well-designed models. The third failure mode, global buckling, occurs when the height-to-width H / w ratio of the wall is greater than 22 with the arranging both bolts and T-stiffeners connectors, as depicted in Fig. 10(c). In this case, out-of-plane deformation happens, especially when the wall height reaches 3000mm, leading to several buckling strips along the length of the wall. This global buckling is more likely when the wall is taller relative to its width, and it results in a noticeable deflection under axial load. However, the steel faceplates and connectors continue to provide confinement to the concrete core, mitigating the severity of this failure mode and protecting the wall from large-scale deflections.

The findings from the FE simulations highlight critical failure modes in DSCSWs and provide valuable insights for improving the design and structure of these systems. To prevent concrete crushing failure, it is essential to ensure adequate confinement of the concrete core using high-performance shear connectors, which can increase the axial load-bearing capacity. Enhancing the connection between the steel plates and concrete core is vital in terms of steel faceplate buckling. This can be achieved by using more robust connectors, such as T-stiffeners or headed studs, which improve the steel-concrete bond and prevent excessive deformation of the faceplates. Lastly, global buckling can be mitigated by optimizing the height-to-width ratio of the shear wall to maintain a balance between the wall's stiffness and its ability to resist axial loads.

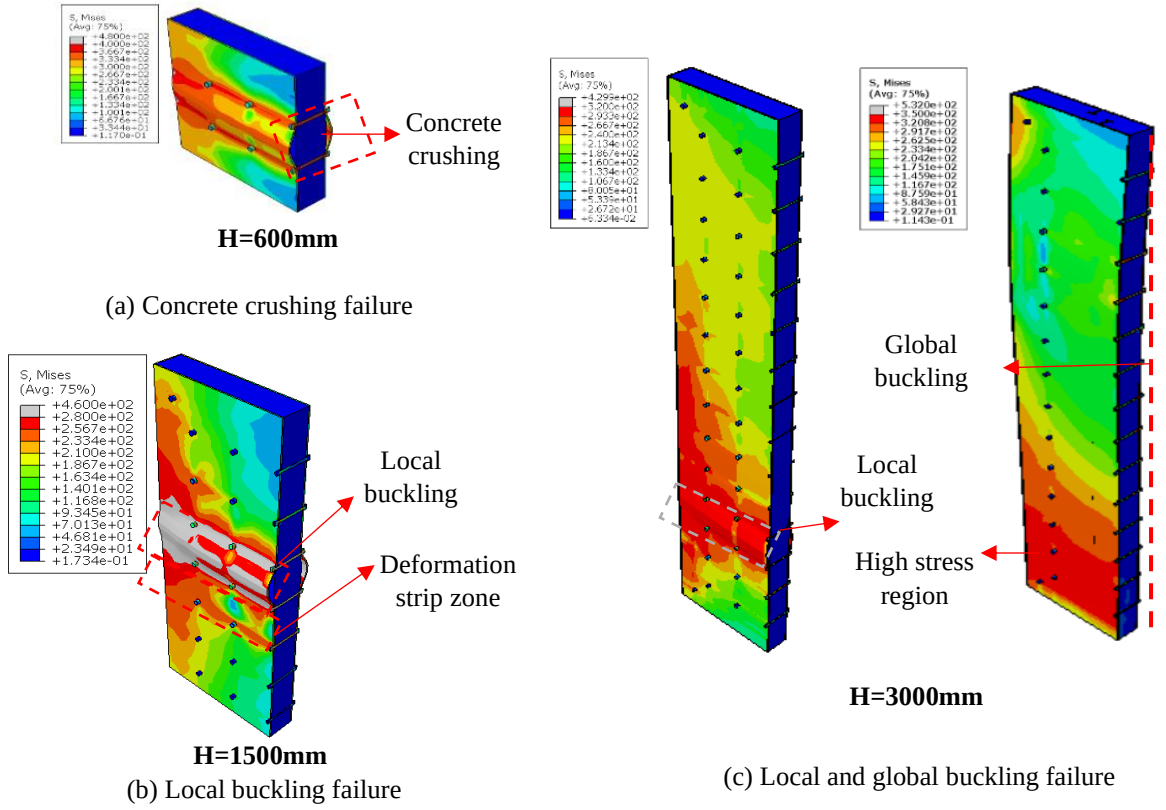

Fig. 10 FE Failure modes of DSCSWs

5. Discussions of parametric analyses

Based on the verified models, FE parametric analyses were operated to examine the impact of five factors on the compressive behavior of DSCSWs. These factors include the type of connectors, wall height, steel plate thickness, bolt connector spacing, and concrete core thickness. This section will examine the influence of these parameters on ultimate compressive capacity, initial stiffness, ultimate vertical displacement, and ductility index.

5.1. Effect of different types of connectors

Three types of connectors were used in this research: bolts, headed studs, and T-stiffeners. These connectors were installed in the FE models across four scenarios: bolts, headed studs, bolts with headed studs, and bolts with T-stiffeners, as presented in Fig. 11(a). The ultimate compressive capacity and ductility index increased with the use of bolts, headed studs, bolts with headed studs, and bolts with T-stiffeners. Among these, bolts, headed studs, and T-stiffeners provided higher ultimate capacity, stiffness, and ductility index compared to bolt connectors. Specifically, the ultimate compressive capacity slightly increased when bolts and headed studs were used separately. However, using bolts with headed studs and bolts with T-stiffeners increased the compressive capacity by 1.9% and 7.1%, respectively. In terms of initial stiffness, the value was 10424 kN/mm when bolts were used. This gradually increased by 2.65% with headed studs and by 3.54% with bolts with headed studs. A significant increase of 18.29% was observed when bolts with T-stiffeners were used. Additionally, the ductility index showed a substantial increase, following the order: 1.22, 1.49, 1.82, and 2.43. These results suggest that the initial stiffness, ductility index, and ultimate compressive capacity of DSCSWs are primarily influenced by the steel plates and the material's resistance. It can be concluded that installing bolts with T-stiffener connectors provides comparable composite action and structural performance to other types of connectors. Therefore, bolts with T-stiffeners are highly recommended for use in composite structures. Furthermore, as shown in Fig. 11(b), T-stiffener connectors resulted in less vertical displacement compared to other connectors, with reductions of approximately 6.67%, 14%, and 16.41% compared to bolts, headed studs, and bolts with headed studs, respectively. Consequently, it can be concluded that bolts with T-stiffener connectors offer comparable compressive behavior to other connectors in terms of vertical displacement, ultimate bearing axial load, initial stiffness, and ductility index. This was further validated by another comparison in this study involving different wall heights, as shown in Figs. 12(a-b) and 13(a-b).

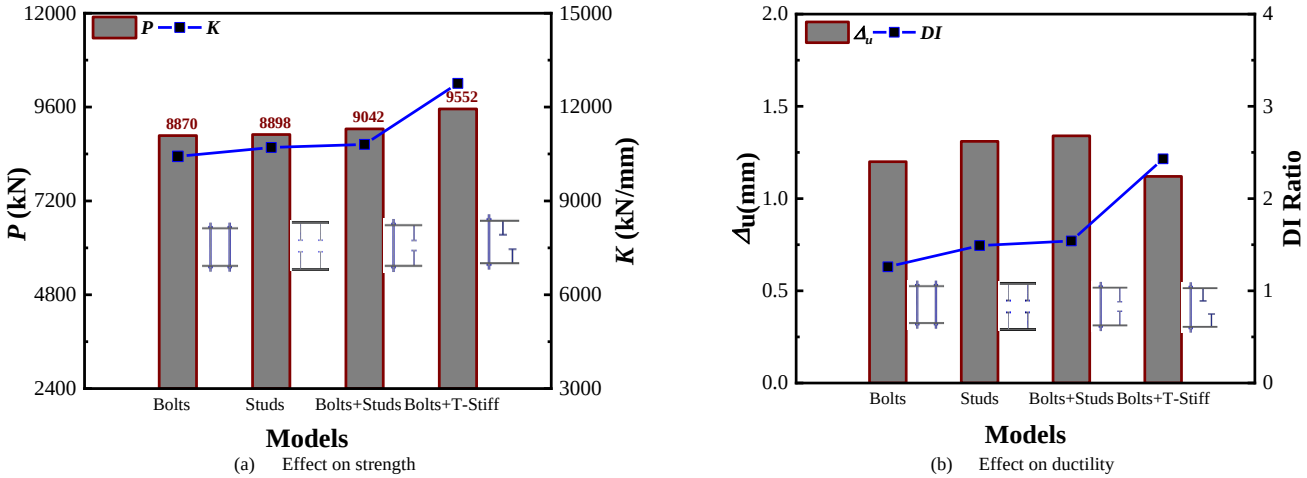

Fig. 11 Effect of different types of connectors on compressive performance with 600mm heights

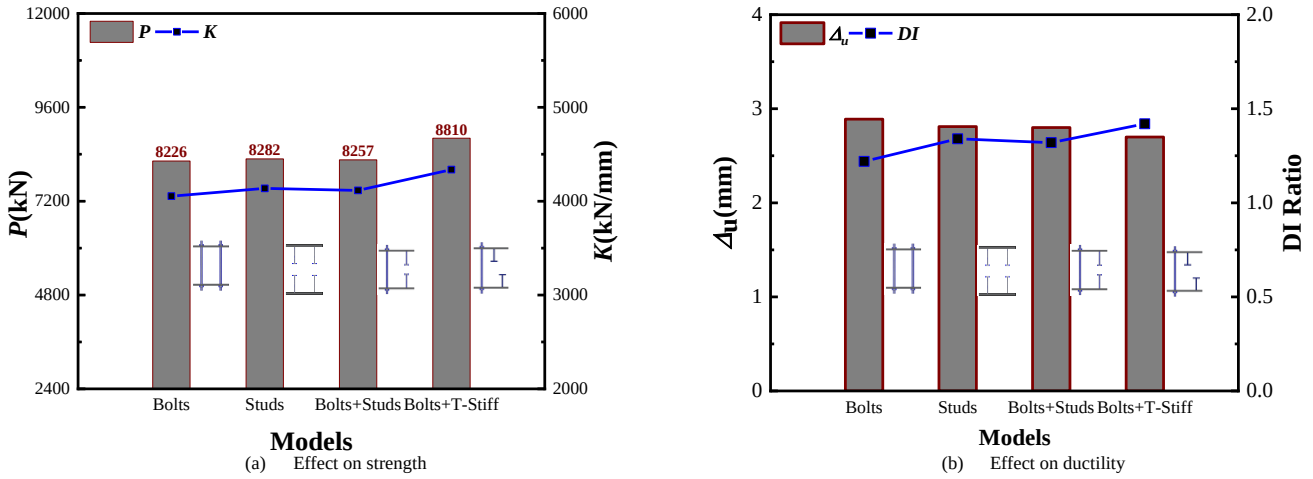

(a) Effect on strength (b) Effect on ductility

Fig. 12 Effect of different types of connectors on compressive performance with 1500mm heights

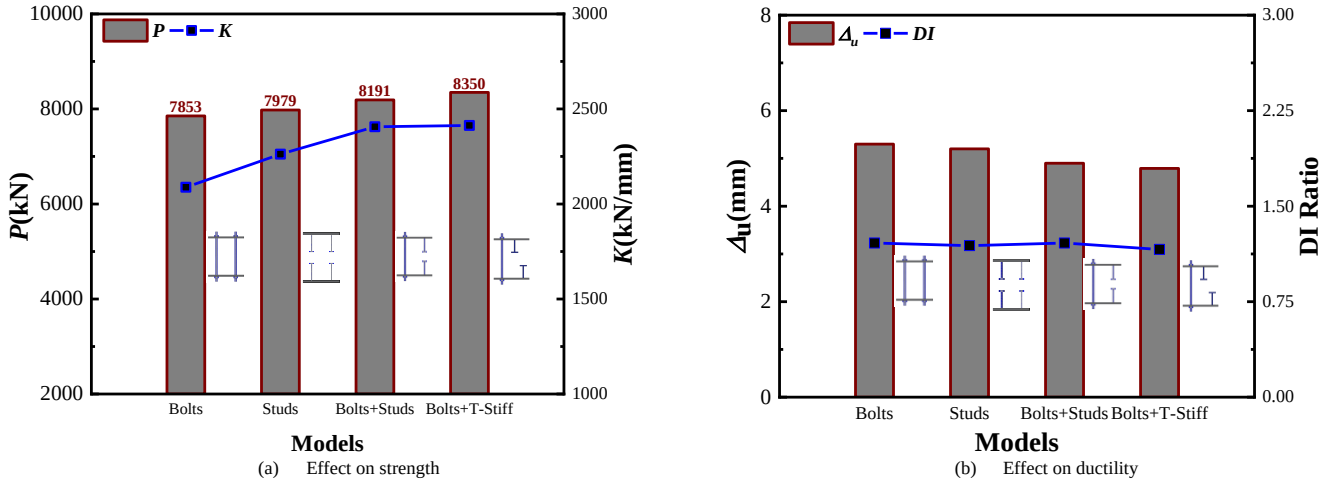

(a) Effect on strength (b) Effect on ductility

Fig. 13 Effect of different types of connectors on compressive performance with 3000mm heights

5.2. Effect height of DSCSW walls

The height of the DSCSWs was modified to study its effect on strength and ductility, as shown in Fig. 14. The results revealed that the ultimate compressive capacity of the walls decreased with increasing height. Similarly, the initial stiffness and ductility exhibited the same trend as the ultimate compressive capacity. In contrast, the vertical displacement increased with the height. Specifically, the ultimate axial compression load was 8870 kN when the height was 600 mm. This value decreased by 7.3% and 11.5% for heights of 1500 mm and 3,000 mm, respectively. The initial stiffness was 10424 kN/mm for the 600 mm height, but it significantly decreased by 61.1% and 79.9% for the 1500 mm and 3000 mm heights, respectively. Meanwhile, the vertical displacement gradually increased from 1.22 mm at 600 mm height to 2.83 mm and 5.30 mm at 1,500 mm and 3,000 mm, respectively, as shown in Fig. 14. Thus, height has a major impact on the ultimate compressive capacity, initial stiffness, ductility, and displacement of the walls, as the models are more likely to fail due to global and local buckling with increasing height, as shown in Fig. 14. These results have been not only numerically validated but also experimentally verified (see Fig. 7(a-e) and Table 4).

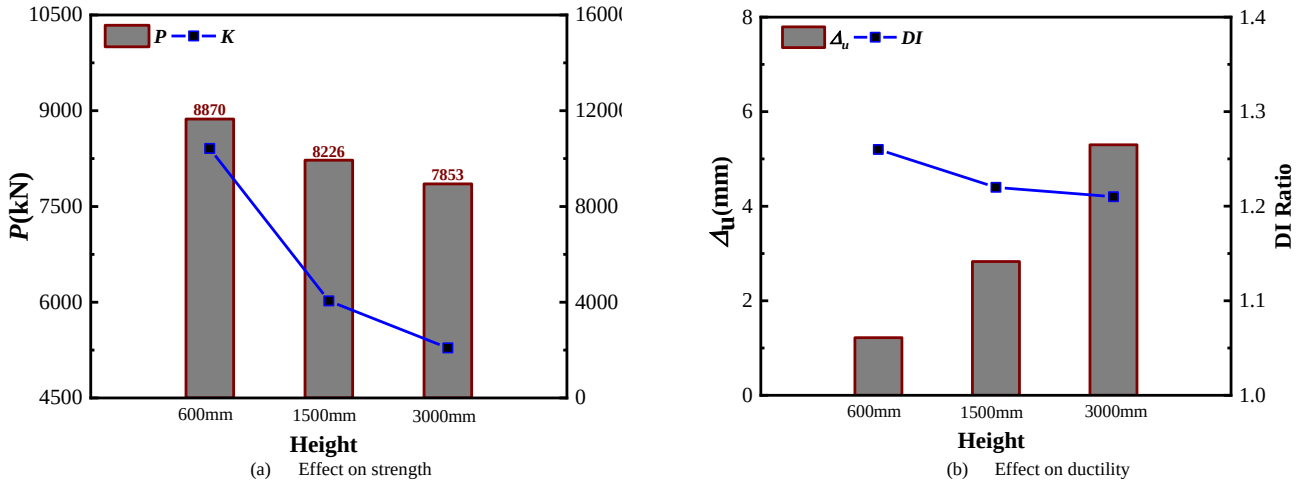

(a) Effect on strength (b) Effect on ductility

Fig. 14 Effect of heights of the wall on the compressive performance of DSCSW

5.3. Effect of thickness of steel plates

Fig. 15 illustrates the influence of the steel plate thickness on the strength and ductility of DSCSWs. The graph shows that the ultimate compressive capacity increased from 7239 kN to 8105 kN, 8870 kN, 9702 kN, and 10621 kN as the thickness of the steel plates increased from 4 mm to 5 mm, 6 mm, 7 mm, and 8 mm, respectively, as shown in Fig. 15(a). Furthermore, reducing the thickness of the steel plates would lower the confinement of the concrete core due to increased local buckling resistance, directly affecting the wall's stiffness. A thinner steel plate would also negatively affect the tensile strength of the bolt connectors, as reduced plate thickness leads to higher buckling. The initial stiffness of the walls slightly increased with the rising thickness of the steel plates. Specifically, when the steel plate thickness was 4 mm, the initial stiffness was 9010 kN/mm. This increased by 7.8%, 15.7%, 25.2%, and 35.0% for thicknesses of 5 mm, 6 mm, 7 mm, and 8 mm, respectively, as displayed in Fig. 15(a). Additionally, the thickness of the steel faceplate significantly impacted vertical displacement. As the steel plate thickness increased, vertical displacement decreased. For example, with a 4 mm thickness, the vertical displacement was 1.65 mm. However, increasing the thickness to 5 mm, 6 mm, 7 mm, and 8 mm reduced the ultimate vertical displacement to 1.42 mm, 1.26 mm, 1.22 mm, and 1.02 mm, respectively, as shown in Fig. 15(b). On the other hand, the ductility index exhibited an opposite trend to vertical displacement, increasing as the steel plate thickness rose. Specifically, when the steel plate thickness was 4 mm, the ductility index was 0.93%. This value steadily increased to 1.18%, 1.32%, 1.38%, and 1.42% for thicknesses of 5 mm, 6 mm, 7 mm, and 8 mm, respectively, as shown in Fig. 15(b). In conclusion, the thickness of the steel plates has a significant impact on the overall mechanical properties of DSCSWs. Increasing the steel plate thickness enhances the DSCSW's compressive performance by increasing the steel content in the section, improving the system's overall mechanical properties.

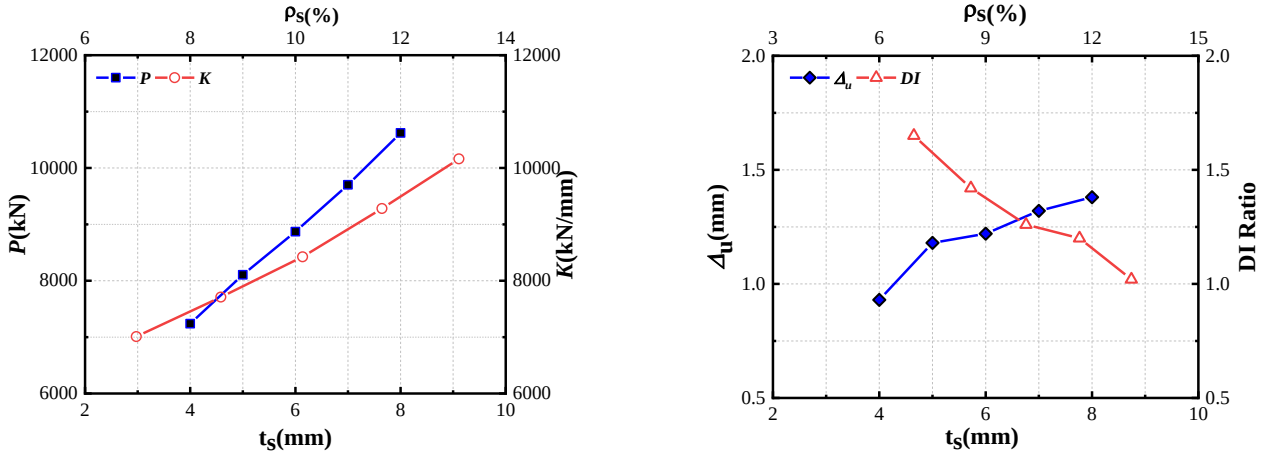

(a) Effect on strength (b) Effect on ductility

Fig. 15 Effect of thickness of steel plates on axial compression behavior of DSCSW

5.4. Effect of spacing of bolt connectors

Different bolt spacing values were used to study the impact of spacing on the overall mechanical properties of DSCSWs under axial compression. Fig. 16 presents the impact of bolt connector spacing on strength and ductility. It can be observed that there is no significant difference in compressive capacity or initial stiffness with varying spacing. Specifically, when the spacing between bolts was 120 mm, the ultimate axial bearing load of the wall was 8425 kN. This value decreased as the spacing increased. When the spacing was adjusted to 160 mm, 200 mm, and 240 mm, the compressive capacity decreased by 1%, 2.4%, and 3.1%, respectively. This reduction is attributed to the increasing slenderness ratio, which rose from 20% to 26.67%, 33.33%, and 40%. Furthermore, increasing the spacing had a minor effect on the initial stiffness of DSCSWs. As the spacing increased from 120 mm to 160 mm, 200 mm, and 240 mm, the initial stiffness values declined from 4200 kN/mm to 4,59 kN/mm, 4054 kN/mm, and 3977 kN/mm, respectively, as illustrated in Fig. 16(a). In addition, Fig. 16(b) illustrates the effect of spacing on the ductility index and ultimate displacement. The graph clearly shows that the ductility index slightly decreased as the bolt spacing increased. Specifically, when the spacing was 120 mm, the ductility index was 1.93%. This value progressively reduced by 31.6%, 36%, and 45.6% for spacings of 160 mm, 200 mm, and 240 mm, respectively. Similarly, the ultimate vertical displacement increased as the ductility index decreased due to the increasing spacing. When the spacing was 120 mm, the ultimate displacement was 2.69 mm. This value increased to 2.89 mm, 2.92 mm, and 3.15 mm for spacings of 160 mm, 200 mm, and 240 mm, respectively. In conclusion, the spacing between bolt connectors has a minor impact on compressive capacity and initial stiffness but significantly affects ultimate vertical displacement and the ductility index.

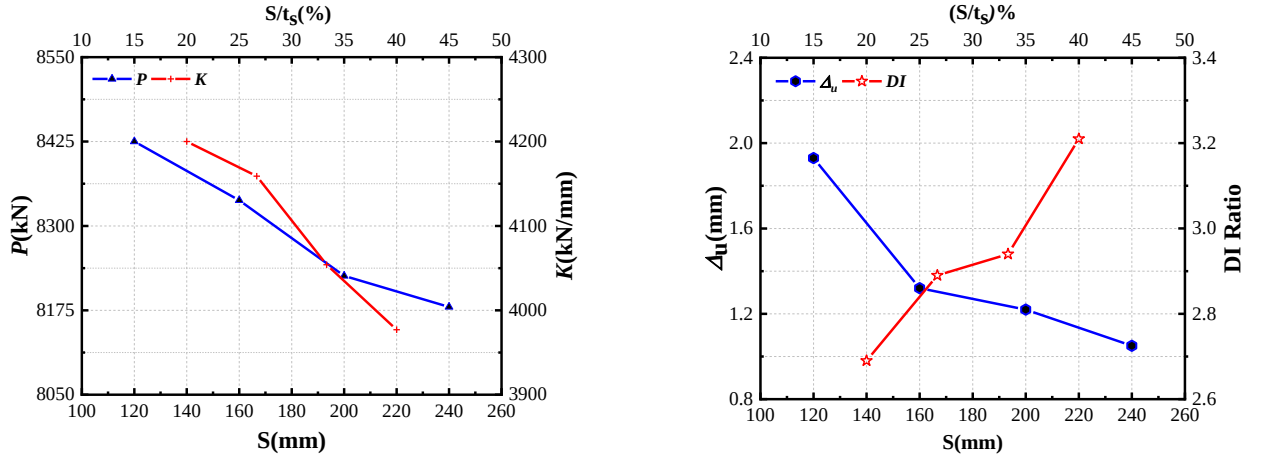

(a) Effect on strength (b) Effect on ductility

Fig. 16 Effect of spacing between bolts connectors on compressive performance DSCSW

5.5. Effect of thickness of the concrete core

Fig. 17 illustrates the effect of thickness of concrete core on the overall compressive stability of DSCSWs. It can be observed that raising the concrete core thickness significantly enhanced both the ultimate compressive capacity and initial stiffness. Specifically, strengthening the core thickness from 98 mm to 108 mm, 118 mm, 128 mm, and 138 mm resulted in a 4.8%, 9.2%, 10.9%, and 12.5% increase in the ultimate compressive capacity of the walls,

respectively. Additionally, the initial stiffness increased with the thickness of the concrete core. More specifically, the initial stiffness rose from 9244 kN/mm to 9861 kN/mm, 10424 kN/mm, 10985 kN/mm, and 11,587 kN/mm, respectively, as shown in Fig. 17(a). This reveals that the concrete core significantly impacts the ultimate compressive capacity and initial stiffness of the wall. It is also evident that the concrete core thickness minimally influences the ultimate vertical displacement and ductility index. The ultimate vertical displacement ranged from 1.12 mm to 1.30 mm, and the ductility index varied from 1.16% to 1.36%, as shown in Fig. 17(b), which can be considered negligible. In conclusion, the core thickness significantly impacts the ultimate compressive capacity and initial stiffness of DSCSWs but has a minor effect on the ductility index and ultimate vertical displacement.

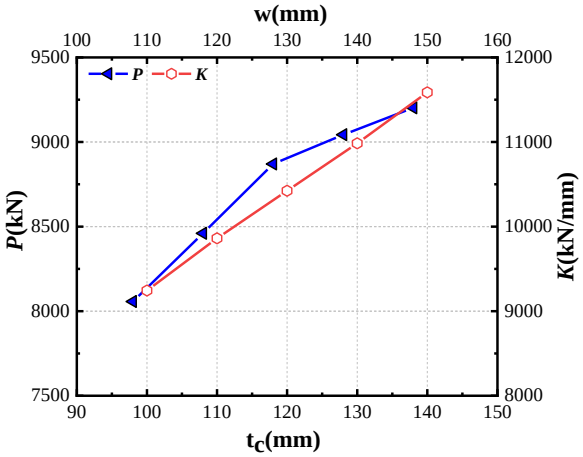

(a) Effect on strength

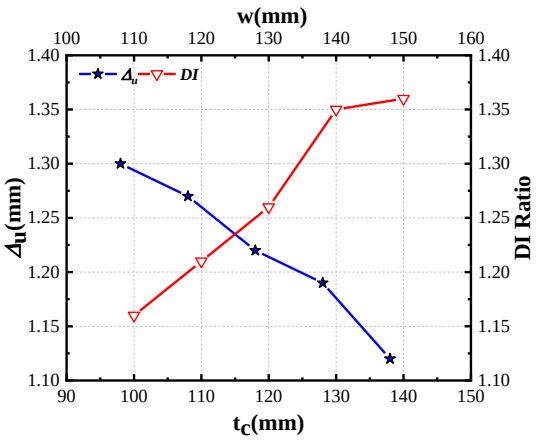

(b) Effect on ductility

Fig. 17 Effect of concrete core' thickness on axial compression behavior of DSCSW

6. Analysis of compressive resistance of DSCSW

6.1. Code methods

In AISC 360 [59], the ultimate compressive capacity of composite structures subjected to axial compression load can be calculated as follows.

$$P_u = \begin{Bmatrix} P_{no}(0.658)^{\frac{P_{no}}{P_e}} \\ 0.877P_e \end{Bmatrix} \quad \text{when} \quad \begin{Bmatrix} P_{no}/P_e \le 2.25 \\ P_{no}/P_e > 2.25 \end{Bmatrix} \tag{8}$$

$$P_{no} = f_y A_s + 0.85 f_c A_c \tag{9}$$

$$P_{cr} = \frac{\pi^2 (EI_{eff})}{(KL)^2} \tag{10}$$

where P_{no} denotes section capacity of DSCSW subjected to axial load and, A_s and A_c are the cross-sectional area of concrete and steel plates, f_y denotes yield strength of steel plates f_c denotes compressive strength of concrete P_{cr} elastic critical buckling load that can be calculated by effective flexural rigidity $(EI_{eff}) = E_s I_s + C_3 E_c I_c$; $C_3 = 0.6 + 2(A_s/A_s + A_c) \le 0.9$, K denotes effective length factor, L is laterally unbraced length of the member.

The ultimate compressive capacity of DSCSW could be determined based on Eurocode 4 [60], as the following

$$P_o = f_y A_s + 0.85 f_c A_c \tag{11}$$

For composite structures, the buckling strength can be predicted by multiplying the section capacity by bucking reduction factor χ

$$P_u = \chi P_o \tag{12}$$

$$\chi = \frac{1}{\varphi + \sqrt{\varphi^2 - \bar{\lambda}^2}} \tag{13}$$

$$\bar{\lambda} = \sqrt{\frac{P_o}{P_{cr}}} \tag{14}$$

$$\varphi = 0.5[1 + \alpha_g(\bar{\lambda} - 0.2) + \bar{\lambda}^2] \tag{15}$$

where P_o is ultimate strength of composite shear wall under compression force, χ reduction factor which is function of the relative slenderness $\bar{\lambda}$ and imperfection, α_g is an imperfection factor corresponding to appropriate buckling curve, and it can be gotten from Table 6.5 in Eurocode 4. P_{cr} elastic critical buckling force that determined by effective flexural rigidity as follow $(EI_{eff}) = E_s I_s + 0.6 E_c I_c$.

6.2. Analytical method

To simplify the ultimate compressive resistance calculations, the following assumptions may be applied.

(1) As DSCSW is composed of steel plates and concrete core, so the ultimate compressive resistance (P_u) provided by the compressive strength of steel (P_s) plates and concrete core (P_c) .

$$P_u = P_c + P_s \tag{16}$$

(2) In the loading stage, the concrete core and steel plates work compositely, and the previous research on composites shears walls showed that the compressive of concrete core P_c can be determined as follows;

$$P_c = \phi A_c \sigma_c \tag{17}$$

where ϕ denotes to reduction factor equals 0.85 according to AISC-360 and Eurocode 4; A_c and σ_c denotes the concrete core's cross-sectional and ultimate compressive capacity, respectively. Yan has suggested a method to calculate (σ_c) in Ref [20].

(3) According to Akiyama [61] study, the yield stress of steel plates can be determined as follows:

$$\sigma_{cr} = \frac{\pi^2 E_s}{12K^2(S/t_s)^2} \tag{18}$$

where E_s Modules of elasticity of steel; S denotes spacing among connectors; t_s denotes the thickness of steel plates; K is the coefficient of effective length, and its value is considered as 0.7 for the safety factor.

In order to investigate the influence of the slenderness ratio of steel plates on the buckling behavior of DSCSWs, Wei et al. [62] conducted buckling analysis and ultimate stress state, and the following equation was suggested to consider the steel plates' buckling stress.

$$\sigma_{cr}=\begin{cases} f_y & ,S/t_s \le \pi\sqrt{E_s/(12K^2 f_y)} \\ \dfrac{\pi E_s}{12K^2(S/t_s)^2} & ,S/t_s > \pi\sqrt{E_s/(12K^2 f_y)} \end{cases} \quad (19)$$

(4) Based on numerical and experimental results on DSCSWs, the type of connectors with steel plates provide confinement to the concrete core and raise the ultimate capacity of composite walls. In contrast, it is noticeable that neither AISC-360 nor Eurocode 4 included the effect of connectors. However, Yan et al. [20] suggested that the steel on the concrete deformation plane could be considered to offer confinement. The confinement stress (σ_h) was defined as an average equal stress allocated across the relevant area, which can be represented by

$$\sigma_h=\frac{T_H}{S^2} \quad (20)$$

where T_H denotes the tensile strength of connectors; S denotes the spacing between two connectors. The tensile resistance of connectors in the DSCSW can be determined according to the degree of confining stress acting on the concrete core. Hence, T_H can be calculated by the equations recommended by Yan at [20, 63-65].

(5) According to test and FE results, the failures of slender DSCSW are inelastic local and global buckling correlating with yielding of steel plates and crushing of concrete core. Therefore, general slenderness and stability of the wall should be taken into considerations, and it can be considered by multiplying the section capacity by stability coefficient (φ) as follows

$$P_u=\varphi P_0 \quad (21)$$

$$\varphi=\begin{cases} 1-0.65\lambda_0^2 \; for \lambda_0 \le 0.215 \\ \dfrac{1}{2\lambda_0^2}[(0.965+0.3\lambda_0+\lambda_0^2)-\sqrt{(0.965+0.3\lambda_0+\lambda_0^2)^2-4\lambda_0^2}] \; for \lambda_0 > 0.215 \end{cases} \quad (22)$$

$$\lambda_0=\frac{l_0}{\pi\sqrt{\dfrac{I_s+I_c E_c/E_s}{A_s+A_c\sigma_c/\sigma_{cr}}}}\sqrt{\frac{\sigma_{cr}}{E_s}} \quad (23)$$

where P_u is ultimate compressive capacity; φ is stability coefficient [66]; λ_0 is generalized slenderness ratio; l_0 is the effective unbraced length of the member; elastic modulus of concrete and steel; I_c and I_s inertia moment of concrete and steel.

6.3. Validations

The ultimate compressive capacity projections are validated with the FE modeling outcomes in Table 5. Fig. 18 shows a scatter plot illustrating the numerical-to-prediction ratio for the results obtained using AISC-360, Eurocode 4, and the analytical method. The mean ratios for AISC-360 and Eurocode 4 are 1.04 and 1.02, respectively, both with the same standard deviation (Std. v) of 0.05. This similarity arises since the criteria in these code methods were initially developed for concrete-filled steel tube columns and do not account for variations in connector types or premature local buckling of steel plates. Additionally, both Table 5 and Fig. 18 reveal that the prediction ratios from these code methods were lower for walls with a height of 600mm, as they were treated as short shear walls. In contrast, the analytical method yields the average percentage of 1.00 with a standard deviation (Std. v) of 0.03. These high mean ratios and low standard deviations emphasize the enhanced accuracy of the analytical method, which incorporates the confinement effect of steel plates and various connector types. Furthermore, Fig. 18 demonstrates that more than 90% of the analytical models fall within the ±5% prediction error range. In conclusion, the analytical method provides reliable estimates of the ultimate compressive capacity for DSCSWs with different connector types.

Table 4
Comparison of ultimate compressive capacity between the numerically and analytically

items	$P_{u,FEM}$	$P_{u,AISC}$	$P_{u,EC4}$	$P_{u,Analytical}$	$P_{u,FE}/P_{u,AISC}$	$P_{u,FE}/P_{u,EC4}$	$P_{u,FE}/P_{u,Analytical}$
DSCSW-1	7239	6970	7035	6993	1.04	1.03	1.04
DSCSW-2	8105	7879	7948	7906	1.03	1.02	1.03
DSCSW-3	8870	8791	8864	8818	1.01	1.00	1.01
DSCSW-4	9702	9705	9783	9732	1.00	0.99	1.00
DSCSW-5	10621	10623	10705	10650	1.00	0.99	1.00
DSCSW-6	9024	8791	8864	8800	1.03	1.02	1.03
DSCSW-7	9552	9359	9442	9387	1.02	1.01	1.02
DSCSW-8	8898	8791	8864	8800	1.01	1.00	1.01
DSCSW-9	8057	8110	8204	8137	0.99	0.98	0.99
DSCSW-10	8460	8452	8534	8478	1.00	0.99	1.00
DSCSW-11	9043	9128	9195	9156	0.99	0.98	0.99
DSCSW-12	9202	9465	9525	9493	0.97	0.97	0.97
DSCSW-13	8425	8416	8482	8613	1.00	0.99	0.98
DSCSW-14	8338	8416	8482	8530	0.99	0.98	0.98
DSCSW-15	8226	8416	8482	8491	0.98	0.97	0.97
DSCSW-16	8186	8416	8482	8469	0.97	0.97	0.97
DSCSW-17	8257	8416	8482	8474	0.98	0.97	0.97
DSCSW-18	8280	8416	8482	8474	0.98	0.98	0.98
DSCSW-19	8810	8937	9004	9020	0.99	0.98	0.98
DSCSW-20	7853	7201	7207	7672	1.09	1.09	1.02
DSCSW-21	8191	7201	7207	7659	1.14	1.14	1.07
DSCSW-22	8350	7580	7548	8111	1.10	1.11	1.03
DSCSW-23	7979	7201	7207	7659	1.11	1.11	1.04
average					1.04	1.02	1.00
Std.v					0.05	0.05	0.03

where $P_{u,FE}$ denotes numerical results of compressive capacity, $P_{u,AISC}$, $P_{u,EC4}$ and $P_{u,Analytical}$ indicate predictions of compressive resistance by AISC-360, Eurocode 4 code and analytical method, respectively.

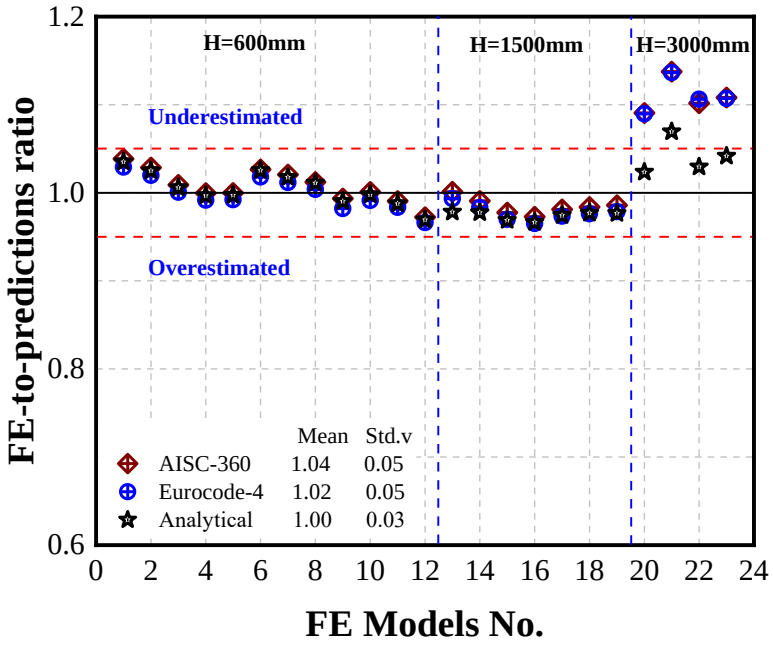

Fig. 18 Comparison between FE analysis results and prediction equations

7. Conclusion

This paper examines the axial compression behavior of DSCSWs. Steel faceplates are prone to buckling between two rows of connectors due to the weak bond between the steel faceplates and the concrete core. To prevent local buckling, separation of steel plates, and to enhance the overall compressive performance of DSCSWs, various methods such as bolts, headed studs, and T-stiffeners have been proposed. In this study, FE modeling was developed and validated with five tested specimens to ensure the accuracy of the results. A parametric analysis was then performed to investigate several key factors based on the verified results. Lastly, the ultimate compressive capacity of DSCSWs was predicted using AISC-360, Eurocode 4, and the analytical method, and the results were compared with those obtained from FE parametric studies. The conclusions drawn from the study are as follows.

(1) The comparison between test and FE modeling results shows that the FE models slightly overestimate both the ultimate compressive capacity and initial stiffness of DSCSWs by 7%. The standard deviations for compressive capacity and stiffness test-to-FE predictions are 0.06 and 0.04, respectively. Discrepancies in the FE models are primarily due to variations in the concrete modulus of elasticity and the loading process. Although the FE models can capture the failure modes including local buckling, concrete crushing and global buckling.

(2) As the wall height increased, the ultimate bearing capacity, initial stiffness, and ductility index showed a decreasing trend, suggesting that height significantly influences the overall performance of DSCSWs. Different types of connectors were also tested, with the results showing that headed studs and T-stiffeners enhanced both compressive capacity and initial stiffness while they reduced the ductility index and vertical displacement. Specifically, using headed studs and T-stiffeners improved axial bearing capacity and stiffness compared to bolt connectors, although ductility slightly decreased with these connectors. Overall, steel faceplate material and connector type play key roles in the performance of DSCSWs, with headed studs and T-stiffeners proving to be more effective than bolt connectors.

(3) The study also identified three primary failure modes in the FE simulations: concrete crushing, steel faceplate buckling, and global buckling. These failure modes emphasize the importance of adequate confinement for the concrete core and the need for robust connections between the steel plates and concrete core to prevent deformation and improve axial load capacity. Furthermore, optimizing the height-to-width ratio of the shear wall is crucial in mitigating global buckling and maintaining overall stability.

(4) T-stiffeners and headed studs significantly improve the compressive capacity, initial stiffness, and ductility of DSCSWs compared to bolts. Combining bolts and T-stiffeners provides the best performance, including reduced vertical displacement. Wall height greatly impacts compressive capacity, stiffness, and displacement, with taller walls showing reduced strength and increased displacement, highlighting a higher risk of buckling. These findings emphasize the importance of selecting appropriate connectors and optimizing height-to-width ratios in DSCSW design to ensure stability and enhanced performance.

(5) The compressive capacity of DSCSWs is substantially impacted by the thickness of the steel plates, the spacing of bolt connectors, and the thickness of the concrete core. Increasing the thickness of the steel plate improves compressive capacity, with values rising as the thickness increases from 4 mm to 8 mm. The concrete core thickness also plays a key role, with greater thicknesses leading to higher compressive capacity. On the other hand, the spacing between bolt connectors has a minor effect on compressive capacity, with only a slight decrease observed as the spacing increases. In conclusion, increasing steel plate thickness and concrete core thickness enhances the compressive capacity of DSCSWs, while bolt connector spacing has a relatively minor impact.

(6) The predictions of ultimate compressive capacity based on the AISC-360-10 code and Eurocode 4 method showed reasonable agreement with the FE results. The average values for these two methods are 1.04 and 1.02, respectively, with the same standard deviation of 0.05. On the other hand, the analytical method was proposed to predict the ultimate compressive capacity of DSCSWs by considering the confinement effect of steel faceplates and different types of connectors. The mean value of this method is 1.00, with a standard deviation of 0.03. Therefore, this method provides acceptable results and can be used for design purposes.

Acknowledgment

The Key Laboratory of New Technology supported this research for the Construction of Cities in Mountain Area (Grant No. LNTCCMA-20240116). The authors also appreciate the fundings from The National Natural Science Foundation of China (Grant No. 52378176) and the S&T Program of Hebei (Grant No. 22375409D).

References

[1] J. Shin and S. Park, "Optimum retrofit strategy of FRP column jacketing system for non-ductile RC building frames using artificial neural network and genetic algorithm hybrid approach," *Journal of Building Engineering*, vol. 57, p. 104919, 2022.

[2] T. Kim and J. M. LaFave, "Proposed new equivalent lateral force design method for low-rise reinforced concrete wall-frame mixed building systems," *Engineering Structures*, vol. 152, pp. 87-101, 2017.

[3] L.-H. Han, W. Li, and R. Bjorhovde, "Developments and advanced applications of concrete-filled steel tubular (CFST) structures: Members," *Journal of constructional steel research*, vol. 100, pp. 211-228, 2014.

[4] Z.-H. Chen, R. Ma, Y.-S. Du, and M. Lian, "Experimental and Theoretical Research on Rcft Beam-Columns Fabricated with Q420b High-Strength Steel Subjected To Eccentric Load," *ADVANCED STEEL CONSTRUCTION*, vol. 16, no. 4, pp. 287-296, 2020.

[5] M. Amer, Z. Chen, Y. Du, W. Mashrah, and W. Zhang, "Experimental and numerical investigations on cyclic performance of L-shaped-CFT column frame-buckling restrained and unrestrained steel plate shear walls with partial double-side/four corner connections," *Journal of Building Engineering*, p. 107568, 2023.

[6] A. Mohammed, Y. Du, Z. Chen, and J. Huang, "Research on Seismic Behavior of CFT-Frame-Buckling Restrained Steel Plate Shear Wall Structures Using Recycled Aggregate Concrete," in *Proceedings of The 17th East Asian-Pacific Conference on Structural Engineering and Construction, 2022: EASEC-17, Singapore*, 2023: Springer, pp. 140-151.

[7] Z. Chen, M. Amer, Y. Du, W. Mashrah, B. Zhao, and J. Huang, "Experimental and numerical study on seismic performance of square and l-shaped Concrete-filled steel tubes column Frame-Buckling steel plate shear walls," *Engineering Structures*, vol. 274, p. 115155, 2023.
[8] Y. Du, M. Amer, Z. Chen, M. Al-Haaj, and J. Huang, "Seismic behaviors of CFT-column frame-four-corner bolted connected buckling-restrained steel plate shear walls using ALC/RAC panels," *Thin-Walled Structures*, vol. 195, p. 111365, 2024.
[9] J. Zhou, P. Li, and N. Guo, "Seismic performance assessment of a precast concrete-encased CFST composite wall with twin steel tube connections," *Engineering Structures*, vol. 207, p. 110240, 2020.
[10] B. Wang, H. Jiang, and X. Lu, "Seismic performance of steel plate reinforced concrete shear wall and its application in China Mainland," *Journal of Constructional Steel Research*, vol. 131, pp. 132-143, 2017.
[11] Y. Zhang, Y. Du, Z. Chen, J. Wang, Y. Xu, and G. Liu, "Research on seismic performance of ITRAC-filled double steel plate composite shear wall," *Journal of Building Engineering*, p. 107073, 2023.
[12] Y. Zhang, Y. Du, Z. Chen, Y. Liu, and W. Zhang, "Material properties of ITRAC and cyclic behavior of double steel plate composite shear wall filled with ITRAC," *Construction and Building Materials*, vol. 394, p. 131635, 2023.
[13] Y. Du, C. Shi, Z. Zhao, Y. Zhang, and T. Li, "Compressive behavior of an innovative double-steel-plate composite shear wall with iron tailings and recycled aggregate concrete," *Journal of Building Engineering*, vol. 91, p. 109523, 2024.
[14] J.-B. Yan, E.-C. Kang, and J. Xie, "BEHAVIOURS OF STEEL-CONCRETE COMPOSITE BEAMS AT LOW TEMPERATURES: MATERIALS AND STRUCTURES," 2023.
[15] J.-G. Nie, H.-S. Hu, J.-S. Fan, M.-X. Tao, S.-Y. Li, and F.-J. Liu, "Experimental study on seismic behavior of high-strength concrete filled double-steel-plate composite walls," *Journal of Constructional Steel Research*, vol. 88, pp. 206-219, 2013.
[16] M. Takeuchi, M. Narikawa, I. Matsuo, K. Hara, and S. Usami, "Study on a concrete filled structure for nuclear power plants," *Nuclear engineering and design*, vol. 179, no. 2, pp. 209-223, 1998.
[17] S. K. Clubley, S. S. Moy, and R. Y. Xiao, "Shear strength of steel–concrete–steel composite panels. Part I—testing and numerical modelling," *Journal of Constructional Steel Research*, vol. 59, no. 6, pp. 781-794, 2003.
[18] Q. Zhao, Y. Li, and Y. Tian, "Cyclic behavior of double-skin composite walls with flat and corrugated faceplates," *Engineering Structures*, vol. 220, p. 111013, 2020.
[19] Y. Qin, G.-P. Shu, G.-G. Zhou, J.-H. Han, and X.-L. Zhou, "Truss spacing on innovative composite walls under compression," *Journal of Constructional Steel Research*, vol. 160, pp. 1-15, 2019.
[20] J.-B. Yan, Z. Wang, Y.-B. Luo, and T. Wang, "Compressive behaviours of novel SCS sandwich composite walls with normal weight concrete," *Thin-Walled Structures*, vol. 141, pp. 119-132, 2019.
[21] K. Kang, "Blast resistance of steel-concrete composite structures," Ph. D. thesis, Department of Civil & Environmental Engineering, National …, 2012.
[22] K. Sohel and J. R. Liew, "Behavior of steel–concrete–steel sandwich slabs subject to impact load," *Journal of Constructional Steel Research*, vol. 100, pp. 163-175, 2014.
[23] M. Xie and J. Chapman, "Developments in sandwich construction," *Journal of Constructional Steel Research*, vol. 62, no. 11, pp. 1123-1133, 2006.
[24] Z.-Y. Huang, J.-Y. Wang, J. R. Liew, and P. W. Marshall, "Lightweight steel–concrete–steel sandwich composite shell subject to punching shear," *Ocean Engineering*, vol. 102, pp. 146-161, 2015.
[25] J. R. Liew and T. Wang, "Novel steel-concrete-steel sandwich composite plates subject to impact and blast load," *Advances in Structural Engineering*, vol. 14, no. 4, pp. 673-687, 2011.
[26] Xiong *et al.*, "Structural behaviour of double skin composite system using ultra-lightweight cement composite," *Construction and Building Materials*, 2015.
[27] Z. Wang, J.-B. Yan, and X.-M. Liu, "NUMERICAL AND THEORETICAL STUDIES ON DOUBLE STEEL PLATE COMPO-SITE WALLS UNDER COMPRESSION AT LOW TEMPERATURES," *Advanced Steel Construction*, vol. 17, no. 4, pp. 376-384, 2021.
[28] B.-J. Choi, C.-K. Kang, and H.-Y. Park, "Strength and behavior of steel plate–concrete wall structures using ordinary and eco-oriented cement concrete under axial compression," *Thin-Walled Structures*, vol. 84, pp. 313-324, 2014.
[29] Y. Yang, J. Liu, and J. Fan, "Buckling behavior of double-skin composite walls: An experimental and modeling study," *Journal of Constructional Steel Research*, vol. 121, no. Jun., pp. 126-135, 2016.
[30] J.-B. Yan, X.-T. Wang, and T. Wang, "Compressive behaviour of normal weight concrete confined by the steel face plates in SCS sandwich wall," *Construction and Building Materials*, vol. 171, pp. 437-454, 2018.
[31] Z. Chen, Y. Jiang, X. Zhang, Q. Yang, and W. Li, "Research on resilience model of steel tube bundle composite shear wall," *Earthq. Eng. Dyn*, vol. 37, pp. 115-122, 2017.
[32] X. Zhang, Y. Qin, and Z. Chen, "Experimental seismic behavior of innovative composite shear walls," *Journal of Constructional Steel Research*, vol. 116, pp. 218-232, 2016.
[33] W. He *et al.*, "Experimental study on seismic behaviors of the welded L-shaped double steel plate-concrete composite shear wall," *Journal of Constructional Steel Research*, vol. 187, p. 106944, 2021.
[34] W. He, Y. Wan, Y. Li, and L. Chen, "Development Research of the Double "L" Shaped Steel Plate-Concrete Composite Shear Wall," in *IOP Conference Series: Earth and Environmental Science*, 2021, vol. 719, no. 2: IOP Publishing, p. 022039.
[35] Y. Du, Y. Zhang, H. Liu, L. Wang, and M. Fu, "Behaviors of restrained rectangular high-strength CFT column under elevated temperature," *Construction and Building Materials*, vol. 432, p. 136616, 2024.
[36] J.-B. Yan, Z. Wang, and X. Wang, "Behaviour of steel-concrete-steel sandwich plates under different ice-contact pressure," *Advanced Steel Construction*, vol. 15, no. 1, pp. 116-122, 2019.
[37] M. Amer, Z.-H. Chen, Y.-S. Du, W. Mashrah, Y.-T. Zhang, and M.-W. Wei, "Research on seismic behavior of L-shaped concrete-filled steel tubes column frame-buckling restrained steel plate shear walls," *ADVANCED STEEL CONSTRUCTION*, vol. 19, no. 3, pp. 273-292 2023.
[38] M. Amer, Y. Du, Z. Chen, S. A. Laqsum, and Y. Zhang, "Seismic behavior of concrete-filled steel tubes column frame-buckling restrained steel plate shear walls connected with bolt/weld," *Thin-Walled Structures*, vol. 189, p. 110911, 2023.
[39] J.-K. Tan *et al.*, "Finite element modelling and design of steel plate shear wall buckling-restrained by hat-section cold-formed steel members," *Journal of Constructional Steel Research*, vol. 174, p. 106274, 2020.
[40] C.-H. Li, J.-B. Yan, H.-N. Guan, and H.-L. Wang, "Numerical study on shear behaviour of enhanced C-channels in steel-UHPC-steel sandwich structures," *ADVANCED STEEL CONSTRUCTION*, vol. 17, no. 3, pp. 253-263, 2021.
[41] S. Guezouli and A. Lachal, "Numerical analysis of frictional contact effects in push-out tests," *Engineering Structures*, vol. 40, pp. 39-50, 2012.
[42] O. Mirza and B. Uy, "Effects of the combination of axial and shear loading on the behaviour of headed stud steel anchors," *Engineering Structures*, vol. 32, no. 1, pp. 93-105, 2010.
[43] M. Pavlović, Z. Marković, M. Veljković, and D. Buđevac, "Bolted shear connectors vs. headed studs behaviour in push-out tests," *Journal of Constructional Steel Research*, vol. 88, pp. 134-149, 2013.
[44] J. Qureshi, D. Lam, and J. Ye, "Effect of shear connector spacing and layout on the shear connector capacity in composite beams," *Journal of constructional steel research*, vol. 67, no. 4, pp. 706-719, 2011.
[45] J.-B. Yan, J. Fan, R. Ding, and X. Nie, "Steel-concrete-steel sandwich composite structures: A review," *Engineering Structures*, vol. 302, p. 117449, 2024.
[46] Z. Huang and J. R. Liew, "Compressive resistance of steel-concrete-steel sandwich composite walls with J-hook connectors," *Journal of Constructional Steel Research*, vol. 124, pp. 142-162, 2016.
[47] J.-B. Yan and W. Zhang, "Numerical analysis on steel-concrete-steel sandwich plates by damage plasticity model: From materials to structures," *Construction and Building Materials*, vol. 149, pp. 801-815, 2017.
[48] *GB/T 50081, Ordinary Concrete Mechanices Performance Test Method Standard, 2019*. (In Chinese).
[49] Wuyapeng, "Experimental Axial Compression Stability of Thin Double Steel-Concrete Composite Shear Wall," Master Academic, 2018-019, Tianjin University, Tianjin, 2019.
[50] H. David, "ABAQUS standard user's manual (Version 6.12. 1)," ed: USA, 2012.
[51] C. S. D. Specifications, "GB50010-2010," *China Building Industry Press: Beijing, China*, 2011.
[52] Y. Du, C. Shi, S.-B. Kang, M. Amer, B. Zhao, and Y. Zhang, "Eccentric compression behaviors of iron tailings and recycled aggregate concrete-filled steel tube columns," *Journal of Constructional Steel Research*, vol. 223, p. 109070, 2024.
[53] Liew, J., Y., Richard, Huang, and Zhenyu, "Numerical studies of steel-concrete-steel sandwich walls with J-hook connectors subjected to axial loads," *Steel & Composite Structures An International Journal*, 2016.
[54] J.-B. Yan, H.-N. Guan, Y.-Y. Yan, and T. Wang, "Numerical and parametric studies on SCS sandwich walls subjected to in-plane shear," *Journal of Constructional Steel Research*, vol. 169, p. 106011, 2020.
[55] X. Liu, Z. Chen, Y. Du, M. Amer, Q. Zhang, Y. Li, J. Chen, "Experimental and theoretical studies on lateral behavior of prefabricated composite concrete-filled steel tubes truss column," *Structures*, vol. 66, p. 106920 2024.
[56] C.-H. Li, J.-B. Yan, and H.-N. Guan, "Finite element analysis on enhanced C-channel connectors in SCS sandwich composite structures," in *Structures*, 2021, vol. 30: Elsevier, pp. 818-837.
[57] J.-B. Yan, A. Chen, and T. Wang, "Compressive behaviours of steel-UHPC-steel sandwich composite walls using novel EC connectors," *Journal of Constructional Steel Research*, vol. 173, p. 106244, 2020.
[58] A. Committee, "Seismic provisions for structural steel buildings (AISC 341-10)," *American Institute of Steel Construction, Chicago-Illinois*, 2010.
[59] A. ANSI, "AISC 341-10," *Seismic provisions for structural steel buildings. Chicago (IL): American Institute of Steel Construction*, 2010.
[60] C. R. Hendy and R. P. Johnson, *Designers' Guide to Eurocode 4: Design of Composite Structures EN 1994-2*. Thomas Telford, 2006.
[61] H. Akiyama, H. Sekimoto, M. Fukihara, K. Nakanishi, and K. Hara, "A compression and shear loading tests of concrete filled steel bearing wall," 1991.
[62] W. Fang-fang, Z. Ze-jun, Y. Jun, and W. Yong-quan, "Computational method for axial compression capacity of double steel-concrete composite shear walls with consideration of buckling," *Engineering Mechanics*, vol. 36, no. 2, pp. 154-164, 2019.
[63] J. Yan, J. Liew, and M. Zhang, "Tensile resistance of J-hook connectors in SCS sandwich composite structure," *J Constr Steel Res*, vol. 100, pp. 146-162, 2014.
[64] J.-B. Yan, J.-Y. Wang, J. R. Liew, X. Qian, and L. Zong, "Ultimate strength behaviour of steel–concrete–steel sandwich plate under concentrated loads," *Ocean Engineering*, vol. 118, pp. 41-57, 2016.
[65] J.-B. Yan, J. R. Liew, X. Qian, and J.-Y. Wang, "Ultimate strength behavior of curved steel–concrete–steel sandwich composite beams," *Journal of Constructional Steel Research*, vol. 115, pp. 316-328, 2015.
[66] CECS-159:2004, "Technical specifications for steel tube concrete structures," no. 8, pp. 35-41, 2004 (In Chinese).